Coverage Analysis for 2D/3D Millimeter Wave Peer-to-Peer Networks

Massimiliano Comisso, *Member, IEEE*, and Fulvio Babich, *Senior Member, IEEE*

***Abstract*— This paper presents a theoretical analysis for estimating the coverage probability in two-dimensional (2D) and three-dimensional (3D) peer-to-peer (P2P) millimeter-wave (mmWave) wireless networks. The analysis is carried out by adopting suitable link state models and realistic propagation conditions, involving path-loss attenuation, angular dispersion, mid- and small-scale fading, which comply with recent channel measurements. The presented framework accounts in detail for the actual shape of the transmitting/receiving antenna patterns and for the spatial statistic that describes the node location, by considering the widely adopted Poisson point process, the uniform distribution, and the random waypoint mobility model. Analytical expressions for the statistic of the received power and simple integral formulas for the coverage probability in the presence of interference and noise are derived. The accuracy of the obtained estimations and of the introduced approximations is checked by independent Monte Carlo validations. As possible applications in the 3D mmWave context, the conceived mathematical theory is used to discuss the impact of the interference model on the reliability of the noise-limited approximation, and to estimate the average link capacity of an interfered P2P communication.**

***Index Terms*— Millimeter-wave network, peer-to-peer, 2D/3D modeling, coverage analysis.**

I. Introduction

THE current proposals for the forthcoming fifth-generation (5G) cellular network have almost univocally identified the millimeter-wave (mmWave) spectrum, between 30 and 300 GHz, as the leading candidate for facing the ever growing capacity demand of wireless access services [1]. This choice is due to two main reasons. Firstly, the larger amount of available bandwidth in the extremely high frequency (EHF) band with respect to the conventional L and S ones so far employed by the 2-4G microwave (μWave) systems. Secondly, the encouraging results achieved by recent channel measurements at 28 and 73 GHz [2]–[6], which have proved the feasibility of mmWave cellular communications, provided that sufficiently small cells and directional antennas are adopted. These reasons are reinforced by the previous release from IEEE of the 802.15.3c, 802.11ad, and 802.16.1 amendments for exploiting the EHF band in wireless personal and local area networks [7], [8], as well as for fixed broadband wireless access [9].

Two distinctive but related features characterize the mmWave communications with respect to the μWave ones: a higher path-loss attenuation, and the possibility of compensating it through miniaturized multi-antenna systems. Both these features derive from the smaller involved carrier wavelengths, which, on one hand, allow the packaging of many antennas on a single device to obtain a high array gain, but, on the other hand, make the communications more sensitive to blockages due to obstacles, thus determining significant differences between line-of-sight (LOS) and non-LOS (NLOS) propagation environments. These aspects depict a challenging network scenario, whose complete theoretical characterization is still in progress, but that can already rely on significant frameworks for the estimation of the achievable performance.

A. Related Work

A detailed two-dimensional (2D) analysis for 60 GHz LOS links is developed in [10], by adopting a Poisson point process (PPP) to model the node location and a linear array of flat-top elements to model the antenna pattern. The analysis does not include fading, but interestingly proves that a not too dense mmWave network remains noise-limited as far as the antennas are sufficiently directional. A PPP-based ultra-dense, and hence interference-limited, 2D mmWave LOS/NLOS scenario is addressed in [11], where the coverage probability obtained in the absence of shadowing using a flat-top antenna is exploited to derive a simplified dense network model. A realistic broadside array pattern is adopted in [12] to analyze, still neglecting shadowing effects, the uplink capacity in 2D and three-dimensional (3D) mmWave NLOS scenarios with uniformly distributed sources. In [13], a detailed coverage analysis for 2D multi-tier mmWave networks with Poisson-distributed base stations (BSs) is presented. The analysis adopts a flat-top antenna and neglects small-scale fading, but has the merit of relying on a three-state link model and on experimental measurements to realistically describe the propagation channel [3]. The initial access in 2D mmWave networks with LOS links is exhaustively addressed in [14], where the interference management problem is analyzed in the absence of small-scale fading assuming a flat-top antenna and Poisson-distributed BSs. Poisson-distributed transmitters and flat-top antennas are also used in [15], which studies

Manuscriptaccepted May 2, 2019.. This work was supported by the Italian Ministry of University and Research (MIUR) within the project FRA 2018 (University of Trieste, Italy), entitled UBER-5G: Cubesat 5G networks - access layer analysis and antenna system development.

The authors are with the Department of Engineering and Architecture (DIA), University of Trieste, 34127 Trieste, Italy (e-mail: mcomisso@units.it; babich@units.it).

the influence of the access protocol on the transition between noise- and interference-limited regimes, further proposing a novel 2D LOS/NLOS blockage model for mmWave networks in the absence of fading. Two coverage analyses for mmWave networks, not including small-scale fading but using realistic antenna patterns, are presented in [16], which models the 3D mmWave LOS/NLOS scenario assuming a uniform distribution (UD) of the nodes, and in [17], which focuses on the 2D LOS case considering, beside the UD, also the random waypoint (RW) mobility model. The impact of the blockage model on the noise-limited assumption is investigated in [18], where the downlink coverage probability for a 2D PPP-based LOS/NLOS mmWave scenario in the absence of shadowing is estimated using a flat-top pattern. A general channel power distribution, including LOS/NLOS models, fading, and antenna gains, is adopted in [19] to study the performance limits of BS densification in multi-dimensional mmWave networks with Poisson-distributed users. Sinc and cosine patterns are used in [20], which analyzes 2D mmWave LOS/NLOS ad-hoc and cellular networks with Poisson-distributed nodes, proving that, in the absence of shadowing, the coverage probability is lower bounded by a non-decreasing function of the antenna array size. The coverage performance of a 2D PPP-based mmWave LOS/NLOS network is also investigated in [21] assuming a flat-top pattern and neglecting shadowing effects, in order to show that the usage of arrays with few elements guarantees a higher robustness against beam alignment errors.

B. Motivation and Contribution

With reference to this overview, some common aspects may be outlined. Firstly, except from [12], [16], [19], just 2D scenarios are addressed, even if experimentally assessed 3D channel models exist [2]–[6], and 3D coverage analyses not focused on mmWave networks are available [22], [23]. The 3D case may be of particular interest for the 5G context, since the short communication distances and the resulting small cell sizes imply a not negligible probability that a source and a destination lie overground or underground relative to one another. This may hold both for cellular communications, with BSs not necessarily placed on the rooftop but also between the floors of a building, and for peer-to-peer (P2P) communications, which are expected to be supported by 5G devices. Secondly, except from [12], [16], [17], which adopt UDs or RW mobility models to describe the node location in a finite space domain, the other coverage analyses consider PPPs, which have the significant advantage of providing tractable and reliable frameworks when the domain can be assumed infinite. However, real BS/user placements do not in general follow a specific statistic, thus the exploration of different spatial models may help to provide a wider view of the mmWave coverage issue. Thirdly, except from [20], which adopts sinc/cosine antenna patterns, and [12], [16], [17], adopting generic patterns but unrealistically assuming all interferers received with the same gain, simplified flat-top models are assumed in the other developed frameworks for reasons of analytical tractability. This however represents a significant limit, since the real antenna pattern and the resulting gains are determinant to reliably characterize an interfered P2P directional communication. Finally, except from [19], LOS/NLOS models, shadowing, and small-scale fading, are not jointly included in the developed frameworks. One may hence infer from the above considerations that the availability of a 2D/3D mmWave LOS/NLOS coverage analysis including realistic antenna patterns, different spatial statistics, mid- and small-scale fading, still represents an open issue.

This paper presents a mmWave coverage analysis specifically addressing this issue. In particular, the analysis, which models the network behavior in a single time slot, is developed to account for a three-state link model and for the main elements that characterize the propagation environment, including path-loss attenuation, angular dispersion, mid- and small-scale fading, by referring to the channel measurements realized in [2]–[6]. The framework also accounts for realistic patterns, without the need of adopting simplified antenna models, and for the node location, by considering the UD, RW, and PPP spatial statistics. For all these three cases, the cumulative distribution function (cdf) of the received interference power and the coverage probability are derived through simple integral formulas. The accuracy of the obtained estimations and of the introduced approximations is checked by independent Monte Carlo validations. The analysis is finally exploited to investigate the influence of the interference model on the acceptability of the noise-limited assumption, and to derive an approximated closed-form expression for the average capacity of an interfered mmWave P2P link.

The paper is organized as follows. Section II introduces the system model. Section III formulates the addressed problem. Section IV presents the coverage analysis. Section V discusses the results and describes the applications. Finally, Section VI summarizes the main conclusions.

Notation. Throughout the paper the following notation is used: $\mathbb{R}_{>0}$ and $\mathbb{R}_{\geq 0}$ denote the sets of positive and non-negative reals, respectively; δ_{ij} denotes the Kronecker delta; $\delta(x)$ denotes the Dirac delta function; $\lceil x \rceil$ denotes the ceiling function; $\mathbb{1}_{\mathbf{X}}(\mathbf{x})$ denotes the indicator function (i.e., $\mathbb{1}_{\mathbf{X}}(\mathbf{x})=1$ if $\mathbf{x}\in\mathbf{X}$, $\mathbb{1}_{\mathbf{X}}(\mathbf{x})=0$ if $\mathbf{x}\notin\mathbf{X}$); $\Gamma(x)$ denotes the gamma function; $\gamma(\cdot,x)$ denotes the lower incomplete gamma function; $\mathrm{erfc}(x)$ denotes the complementary error function; ${}_iF_j(\cdot;\cdot;x)$ denotes the generalized hypergeometric function with i type-1 parameters and j type-2 parameters; $\mathrm{Bi}(x)$ denotes the Airy function of the second kind.

II. System Model

Consider the problem of evaluating the coverage probability in a single time slot (single snapshot analysis) for a mmWave wireless network in which a destination D lies at the center O of a ball $\mathbf{B}_\nu(O,\bar{R})$ of radius $\bar{R}$ and dimension $\nu\in\mathbb{D}=\{2,3\}$. In this network, L P2P communications are active, thus D receives the power from its desired source and from the other $L-1$ ones that are perceived by D as interferers. The reference systems for $\nu=2$ and $\nu=3$ are reported in Figs. 1(a) and 1(b), respectively, where S_1 identifies the desired source, S_i ($i=2,...,L$) denotes a generic interfering source, and the shaded shapes represent the directional antenna patterns used by the nodes. In particular, S_1 and D steer towards each other the maxima of their patterns to support the target link, while

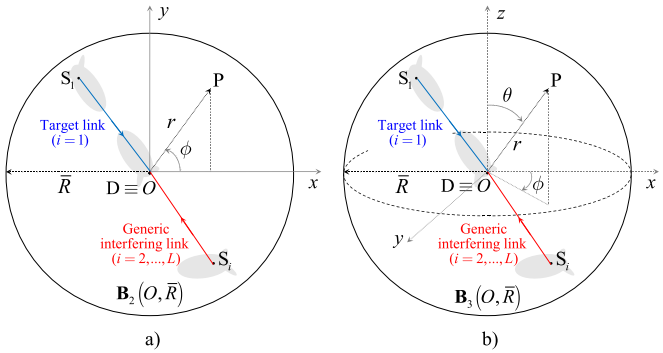

Fig. 1. Reference systems: (a) $\nu = 2$, (b) $\nu = 3$.

the generic interferer steers its pattern towards its intended destination (not reported in the figure), anyway generating an interfering link towards D. All sources adopt an identical transmission power P_{T}. The generic point P with respect to O is defined in polar coordinates by the pair (r, ϕ) in the 2D case and in spherical coordinates by the triad (r, θ, ϕ) in the 3D one, where r denotes the distance, while ϕ and θ represent the azimuth and zenith angles, respectively. Using these reference systems in combination with the spatial statistic of the sources allows the description of the statistical location of $\mathrm{S}_1, ..., \mathrm{S}_L$.

A. Spatial Statistics

Three well-accepted models are considered to describe the location of the sources: the UD [24], the RW model [25], and the homogeneous PPP [22]. These statistics cover a wide set of common scenarios and generate networks with different spatial properties that can lead to different performance.

1) Uniform Distribution: The UD is the most used statistic when a bounded region containing a finite number of nodes has to be taken into account. With reference to the generic point (r, ϕ), denoting the realization of a random vector (rV) (R, Φ), the UD over a disk $\mathbf{B}_2(O, \bar{R})$ can be described by the joint probability density function (pdf) [26]:

$$f_{R,\Phi}^{2,\mathrm{UD}}(r, \phi) = \frac{r}{\pi \bar{R}^2} \mathbb{1}_{[0,\bar{R}]\times\mathbf{T}_2}(r, \phi), \tag{1}$$

where $\mathbf{T}_2 = [0, 2\pi[$. In the 3D case, the realization (r, θ, ϕ) of the rV (R, Θ, Φ) in the presence of a UD over a ball $\mathbf{B}_3(O, \bar{R})$ may be instead described by the joint pdf [16]:

$$f_{R,\Theta,\Phi}^{3,\mathrm{UD}}(r, \theta, \phi) = \frac{3r^2 \sin\theta}{4\pi \bar{R}^3} \mathbb{1}_{[0,\bar{R}]\times\mathbf{T}_3}(r, \theta, \phi), \tag{2}$$

where $\mathbf{T}_3 = [0, \pi] \times [0, 2\pi[$. The marginal pdf of the distance $R = R_i$ $(i = 1, ..., L)$ between a source S_i and the destination D may be obtained for $\nu \in \mathbb{D}$ by integrating (1) on $\mathbf{T}_2$ and (2) on $\mathbf{T}_3$. The result of this operation may be expressed in compact form, for $i = 1, ..., L$, as:

$$f_{R_i}^{\nu,\mathrm{UD}}(r_i) = \frac{\nu r_i^{\nu-1}}{\bar{R}^{\nu}} \mathbb{1}_{[0,\bar{R}]}(r_i), \tag{3}$$

from which the cdf of R_i (distance distribution), may be immediately evaluated as:

$$\begin{aligned} F_{R_i}^{\nu,\mathrm{UD}}(r_i) &= \int_{-\infty}^{r_i} f_{R_i}^{\nu,\mathrm{UD}}(r_i')\mathrm{d}r_i' \\ &= \left(\frac{r_i}{\bar{R}}\right)^{\nu} \mathbb{1}_{[0,\bar{R}]}(r_i) + \mathbb{1}_{]\bar{R},+\infty[}(r_i). \end{aligned} \tag{4}$$

2) Random Waypoint: The RW is a typical mobility model used in network simulators, which, similarly to the UD, considers a constant number of nodes enclosed inside a finite space. In this model, a source S_i uniformly selects a point inside $\mathbf{B}_\nu(O, \bar{R})$ and moves towards it with a random speed uniformly chosen within a predefined interval. Once the point is reached, the source stops moving for a given time, at the end of which a novel point and a novel speed are again randomly selected. When the number of movement periods approaches infinity, one obtains an asymptotic (steady-state) distance distribution, which, for both the 2D and 3D cases, is nonuniform and independent of the speed chosen for the nodes [27]. Under these conditions, the asymptotic pdf of R_i, for $\nu \in \mathbb{D}$ and $i = 1, ..., L$, may be represented as [25], [28]:

$$f_{R_i}^{\nu,\mathrm{RW}}(r_i) = \frac{1}{r_i} \left\{ \sum_{k=1}^{\nu} \zeta_{\nu,k} a_{\nu,k} \left(\frac{r_i}{\bar{R}}\right)^{\zeta_{\nu,k}} \right\} \mathbb{1}_{[0,\bar{R}]}(r_i), \tag{5}$$

where $\zeta_{\nu,k} = [\nu + 2(k-1)]$, while $a_{2,1} = 2$, $a_{2,2} = -1$ [25], and $a_{3,1} = 245/72$, $a_{3,2} = -119/36$, $a_{3,3} = 65/72$ [28]. By integrating (5) with respect to r_i, one obtains the asymptotic distance distribution as:

$$F_{R_i}^{\nu,\mathrm{RW}}(r_i) = \left[\sum_{k=1}^{\nu} a_{\nu,k} \left(\frac{r_i}{\bar{R}}\right)^{\zeta_{\nu,k}} \right] \mathbb{1}_{[0,\bar{R}]}(r_i) + \mathbb{1}_{]\bar{R},+\infty[}(r_i). \tag{6}$$

3) Homogeneous Poisson Point Process: The PPP is a spatial model that is often used when the objective is the derivation of mathematically tractable theoretical frameworks, thanks to the independence assumption regarding the nodes deployed in disjoint areas. With reference to the here considered scenarios, denote as Π the homogeneous PPP on $\mathbb{R}^\nu$ of intensity $L/(K_\nu \bar{R}^\nu)$, with $K_\nu = \pi^{\nu/2}/\Gamma(\nu/2 + 1)$ denoting the volume of the unit ν-ball. Exploiting the thinning property of PPPs [13], Π may be partitioned into L independent PPPs $\Pi_1, ..., \Pi_L$, where Π_i $(i = 1, ..., L)$ describes the location of S_i and is characterized by an intensity $\lambda_1 = 1/(K_\nu \bar{R}^\nu)$. According to [29], the pdf of R_i, for $\nu \in \mathbb{D}$ and $i = 1, ..., L$, is given by:

$$f_{R_i}^{\nu,\mathrm{PPP}}(r_i) = \nu K_\nu \lambda_1 r_i^{\nu-1} \exp(-K_\nu \lambda_1 \, r_i^\nu) \, \mathbb{1}_{\mathbb{R}_{\geq 0}}(r_i). \tag{7}$$

By integrating (7) with respect to r_i, one obtains the distance distribution of S_i as:

$$F_{R_i}^{\nu,\mathrm{PPP}}(r_i) = [1 - \exp(-K_\nu \lambda_1 r_i^\nu)] \, \mathbb{1}_{\mathbb{R}_{\geq 0}}(r_i). \tag{8}$$

Remark 1: The above formulation for the three spatial statistics considers one source at a time and hence an independent distance distribution for each interferer. In this way, the signal incoming from each undesired source may be realistically assumed subject to individual channel realizations. Under this condition, a widely adopted approximation for modeling the total interference received by D consists in taking the power

$$f_{\boldsymbol{\Omega}_{\nu,n}}(\boldsymbol{\omega}_{\nu,n}) = \hat{K}_{\nu,n} \cdot \mathbb{1}_{\mathbf{T}_\nu}(\boldsymbol{\omega}_{\nu,n}) \cdot \begin{cases} \exp\left[-\dfrac{(\phi_n-\pi)^2}{2\hat{\sigma}^2_{\phi,n}}\right] & \nu = 2 \\ \exp\left[-\dfrac{(\phi_n-\pi)^2}{2\hat{\sigma}^2_{\phi,n}} - \dfrac{(\theta_n-\pi/2)^2}{2\hat{\sigma}^2_{\theta,n}}\right] & \nu = 3 \end{cases} \tag{14}$$

incoming from the strongest interferer [12]. This approach will be adopted in the here developed analysis. An alternative strategy is however often applied [13]. This strategy jointly accounts for the $L-1$ undesired sources $\mathrm{S}_2, ..., \mathrm{S}_L$ by considering the nearest one through the rv $R_{\min} = \min(R_2, ..., R_L)$, which represents the distance of the interferer closest to D. The cdf of $R_{\min}$ may be immediately derived for $\nu \in \mathbb{D}$ and $d \in \mathbb{S} = \{\mathrm{UD}, \mathrm{RW}, \mathrm{PPP}\}$ as [30]:

$$F^{\nu,d}_{R_{\min}}(r_{\min}) = 1 - \left[1 - F^{\nu,d}_{R_i}(r_{\min})\right]^{L-1}. \tag{9}$$

For $d = \mathrm{PPP}$, (9) takes a really manageable form, since it becomes equal to (8) evaluated at $\lambda_{L-1} = (L-1)\lambda_1$. Hence, to enable a comparison of the results obtained using the strongest and the nearest interferer approximations, the analysis, in the PPP case, will be developed using a generic intensity $\lambda \in \Lambda = \{\lambda_1, \lambda_{L-1}\}$, thus considering the distance distribution:

$$\tilde{F}^{\nu,\mathrm{PPP}}_R(r;\lambda) = \left[1 - \exp\left(-K_\nu \lambda r^\nu\right)\right] \mathbb{1}_{\mathbb{R}_{\geq 0}}(r), \tag{10}$$

which leads to the pdf:

$$\tilde{f}^{\nu,\mathrm{PPP}}_R(r;\lambda) = \nu K_\nu \lambda r^{\nu-1} \exp(-K_\nu \lambda r^\nu)\, \mathbb{1}_{\mathbb{R}_{\geq 0}}(r), \tag{11}$$

and that provides (8) for $\lambda = \lambda_1$ (i.e., $F^{\nu,\mathrm{PPP}}_{R_i}(r_i) = \tilde{F}^{\nu,\mathrm{PPP}}_R(r_i;\lambda_1)$), and (9) for $\lambda = \lambda_{L-1}$ (i.e., $F^{\nu,\mathrm{PPP}}_{R_{\min}}(r_{\min}) = \tilde{F}^{\nu,\mathrm{PPP}}_R(r_{\min};\lambda_{L-1})$). □

Remark 2: Isotropy may be assumed for all the three spatial statistics. In fact, for UDs and PPPs, this property derives immediately from their definition [13], [26], while, for RW models, the isotropy can be achieved by selecting the starting point of the process as coincident with the origin O [31]. For all the three spatial statistics the direction can be therefore described in the 2D case from (1) by the marginal:

$$f^{2,d}_\Phi(\phi) = \int_{-\infty}^{\bar{R}} f^{2,\mathrm{UD}}_{R,\Phi}(r,\phi)\mathrm{d}r = \frac{1}{2\pi}\, \mathbb{1}_{[0,2\pi[}(\phi), \tag{12}$$

and in the 3D one from (2) by the marginals:

$$f^{3,d}_\Phi(\phi) = \int_{-\infty}^{\bar{R}} \int_0^\pi f^{3,\mathrm{UD}}_{R,\Theta,\Phi}(r,\theta,\phi)\mathrm{d}r\mathrm{d}\theta = f^{2,d}_\Phi(\phi), \tag{13a}$$

$$f^{3,d}_\Theta(\theta) = \int_{-\infty}^{\bar{R}} \int_0^{2\pi} f^{3,\mathrm{UD}}_{R,\Theta,\Phi}(r,\theta,\phi)\mathrm{d}r\mathrm{d}\phi = \frac{\sin\theta}{2}\, \mathbb{1}_{[0,\pi]}(\theta). \tag{13b}$$

Hence, for a given the ν value, UD, RW, and PPP present the same statistic of the direction. Given the 5G densification strategy, isotropy may be assumed acceptable not only in the 2D case, but also in the 3D one, where the sources are expected to be spread both in area and height over buildings, industrial plants, public works (bridges, monuments, ...). In all these cases, it is reasonable to not consider some transmitting directions more likely than others. □

B. Angle and Gain Statistics

According to the 5G proposals, the communications have to be realized adopting directional antenna patterns in transmission and reception to compensate the strong attenuations of the mmWave channel [3]. To address a general but mathematically tractable scenario, the sources are assumed to adopt the same pattern, while the destination can use a pattern different from that employed by the sources. In both cases, the pattern is electronically steered to point its maximum towards the direction of interest. Since L P2P communications are simultaneously active, the result of the target S_1-D one depends not only on the S_1/D maximum transmitting/receiving antenna gains, but also on the transmitting gain of each of the $L-1$ interferers.

To jointly model this situation in the 2D and 3D cases, adopt, for the generic direction, the notation $\boldsymbol{\omega}_\nu \in \mathbf{T}_\nu$ to identify the realization of the rV $\boldsymbol{\Omega}_\nu$, where, for $\nu = 2$, $\boldsymbol{\omega}_2 = \phi \in \mathbf{T}_2$ and $\boldsymbol{\Omega}_2 = \Phi$, while, for $\nu = 3$, $\boldsymbol{\omega}_3 = (\theta,\phi) \in \mathbf{T}_3$ and $\boldsymbol{\Omega}_3 = (\Theta,\Phi)$. According to this notation, $\mathcal{A}_1(\boldsymbol{\omega}_\nu)$ denotes the transmitting antenna power gain of a source (desired or interfering), and $\mathcal{A}_2(\boldsymbol{\omega}_\nu)$ represents the receiving antenna power gain of the destination. The generic pattern $\mathcal{A}_n(\boldsymbol{\omega}_\nu)$, for $n = 1, 2$, may be expressed as the product between the maximum gain $\mathcal{A}^{\max}_n$ and a normalized function $\tilde{\mathcal{A}}_n(\boldsymbol{\omega}_\nu)$ that accounts for the pattern shape. Precisely this shape is one of the two elements that determine the angular distribution of the transmitted/received powers. The other element is the angular dispersion of the channel, which, in transmission ($n = 1$), may be modeled by the pdf $f_{\boldsymbol{\Omega}_{\nu,1}}(\boldsymbol{\omega}_{\nu,1})$ of the direction of departure (DoD) $\boldsymbol{\Omega}_{\nu,1}$, and, in reception ($n = 2$), by the pdf $f_{\boldsymbol{\Omega}_{\nu,2}}(\boldsymbol{\omega}_{\nu,2})$ of the direction of arrival (DoA) $\boldsymbol{\Omega}_{\nu,2}$. These pdfs are commonly assumed Gaussian for $\nu = 2$ and given by the product between two univariate Gaussian pdfs for $\nu = 3$ [2]. Therefore, $f_{\boldsymbol{\Omega}_{\nu,n}}(\boldsymbol{\omega}_{\nu,n})$ may be defined for $\nu \in \mathbb{D}$ and $n = 1, 2$ according to (14), shown at the top of the page, in which $\hat{K}_{\nu,n}$ is a normalization constant, $\hat{\sigma}_{\phi,n}$ is the azimuth angular spread, and $\hat{\sigma}_{\theta,n}$ is the zenith angular spread. To maintain the analytical tractability of the model, (14) is ideally assumed independent of the antennas, thus neglecting the impact, discussed in [2]–[4], of the pattern shape on the actually measured DoD/DoA statistics.

The joint effects of the antenna shape and of the channel angular dispersion may be modeled by the normalized equivalent transmitting ($n = 1$) and receiving ($n = 2$) gains [26]:

$$\mathcal{G}_{\nu,n}(\boldsymbol{\omega}_{\nu,n}) = \int_{\mathbf{T}_\nu} \tilde{\mathcal{A}}_{\nu,n}(\boldsymbol{\omega}'_{\nu,n}) f_{\boldsymbol{\Omega}_{\nu,n}}(\boldsymbol{\omega}'_{\nu,n} - \boldsymbol{\omega}_{\nu,n})\mathrm{d}\boldsymbol{\omega}'_{\nu,n}, \tag{15}$$

which combine the transmitting pattern shape with the statistic of the DoD ($n=1$), and the receiving pattern shape with the statistic of the DoA ($n=2$). Since all nodes use directional patterns, the power received by D from S_i depends on the product between the normalized equivalent transmitting gain of S_i and the normalized equivalent receiving gain of D. From now on, this quantity will be referred to as the equivalent product gain.

Consider (15) from the point of view of D. To support the target S_1-D link, S_1 steers the direction of maximum radiation towards D, and, similarly, D steers the direction of maximum radiation towards S_1. Hence, for the target link, the equivalent product gain is a constant given by $\mathcal{G}_{\nu}^{\max}=\mathcal{G}_{\nu,1}^{\max}\mathcal{G}_{\nu,2}^{\max}$, where $\mathcal{G}_{\nu,n}^{\max} = \max_{\boldsymbol{\omega}_{\nu,n}\in\mathbf{T}_{\nu}} \mathcal{G}_{\nu,n}(\boldsymbol{\omega}_{\nu,n})$ for $n=1,2$. For an interfering link, instead, the direction $\boldsymbol{\omega}_{\nu,n}$ of an incoming interferer is random and in general not coincident with the direction of maximum radiation of D (Fig. 1). Besides, since S_i ($i=2,...,L$) steers its pattern towards its intended destination, thus not necessarily towards D, both $\mathcal{G}_{\nu,1}$ and $\mathcal{G}_{\nu,2}$ are rvs that may be characterized by the pdfs $f_{\mathcal{G}_{\nu,1}}(\mathfrak{g}_{\nu,1})$ and $f_{\mathcal{G}_{\nu,2}}(\mathfrak{g}_{\nu,2})$, respectively. Thus, the equivalent product gain $\mathcal{G}_{\nu}=\mathcal{G}_{\nu,1}\mathcal{G}_{\nu,2}$, when referred to an interfering link, is a rv whose pdf may be derived from the product distribution as [30]:

$$f_{\mathcal{G}_{\nu}}(\mathfrak{g}_{\nu}) = \int_0^1 \frac{f_{\mathcal{G}_{\nu,1}}(\mathfrak{g}_{\nu,1})}{\mathfrak{g}_{\nu,1}} f_{\mathcal{G}_{\nu,2}}\left(\frac{\mathfrak{g}_{\nu}}{\mathfrak{g}_{\nu,1}}\right) \mathrm{d}\mathfrak{g}_{\nu,1}. \tag{16}$$

From a practical point of view, the estimation of $f_{\mathcal{G}_{\nu}}(\mathfrak{g}_{\nu})$ may be carried out by first deriving $f_{\mathcal{G}_{\nu,n}}(\mathfrak{g}_{\nu,n})$, for $n=1,2$, through the method developed in [12], and then numerically solving (16). The relevant advantage of this modeling approach is the availability of a unique pdf that jointly accounts for the real transmitting/receiving pattern shapes, without the need of introducing approximated antenna models, and for the DoD/DoA statistics, by concisely summarizing the effects of the four functions within a unique rv.

Remark 3: The isotropy claimed in *Remark 2* implies that, given $\tilde{\mathcal{A}}_{\nu,n}(\boldsymbol{\omega}_{\nu,n})$ and $f_{\boldsymbol{\Omega}_{\nu,n}}(\boldsymbol{\omega}_{\nu,n})$, the pdf of $\mathcal{G}_{\nu,n}$ is identical for the three considered spatial models. Thus, the estimation of $f_{\mathcal{G}_{\nu,n}}(\mathfrak{g}_{\nu,n})$, for $n=1,2$, and, in turn, that of $f_{\mathcal{G}_{\nu}}(\mathfrak{g}_{\nu})$, requires to use (12) in the 2D scenario, or (13) in the 3D one, regardless of which of the three spatial statistics is taken into account. □

C. Link State Model

Based on the proposal in [3], a three-state statistical link model is assumed. Accordingly, each mmWave link may be in outage (OUT), LOS, or NLOS state. In particular, the OUT state, which becomes significant for large mmWave cells, occurs when the path-loss is too high and hence the link cannot be established. The LOS state instead occurs when the link is not blocked, while the NLOS one when the link is blocked [13]. To obtain a more compact notation, define as H the rv describing the link state, where $h=0,1,2$ identify the OUT, LOS, and NLOS states, respectively. According to [3], the probabilities of being in each state depend on the distance r_i between D and S_i, thus one can define a mapping between r_i and the link state probability [18]. From a mathematical point of view, this mapping may be interpreted as a conditioning, so as to define a conditional probability mass function (pmf) of H given R_i as [3]:

$$f_{H|R_i}(h|r_i) = \begin{cases} \max[0, 1-\exp(-\mathcal{H}_{\mathrm{out}} r_i + \mathcal{K}_{\mathrm{out}})] & h=0 \\ \left[1 - f_{H|R_i}(0|r_i)\right] \exp(-\mathcal{H}_{\mathrm{los}} r_i) & h=1 \\ 1 - \sum_{h=0}^{1} f_{H|R_i}(h|r_i) & h=2 \end{cases} \tag{17}$$

where $\mathcal{H}_{\mathrm{out}}$, $\mathcal{K}_{\mathrm{out}}$, and $\mathcal{H}_{\mathrm{los}}$ are parameters related to the propagation environment that can be derived by fitting of experimental data. In (17), as explained in [3], the outage probability is inferred from the 3GPP suburban relay-UE NLOS model [32], while the LOS probability derives from the random shape theory. The conditioning of (17) implies that $f_{H|R_i}(h|r_i)$ is influenced by the distance distribution, and, in turn, by the spatial statistic of the sources.

D. Propagation Model

In agreement with the measurements realized in [3], the omnidirectional path-loss attenuation $\varrho_h(r_i)$ may be assumed infinite for an OUT link ($h=0$), while can be described for LOS ($h=1$) and NLOS ($h=2$) links by the widely adopted floating-intercept model. This yields:

$$\varrho_h(r_i) = \begin{cases} \infty & h=0 \\ \alpha_h r_i^{\beta_h} & h=1,2 \end{cases} \tag{18}$$

where the pair (α_h, β_h) identifies the path-loss parameters for the corresponding link state. In particular, the path-loss is assumed to linearly depend on the logarithm of the distance, with α_h representing the floating intercept and β_h denoting the average path-loss exponent obtained by a best-fit linear regression of empirical data.

Beside the distance-dependent attenuation, the adopted channel model accounts for the random power variations due to mid- and small-scale fading. More precisely, mid-scale fading, which is significant in mmWave communications, is modeled for LOS and NLOS links by a rv Ξ_h following, for $h=1,2$, a log-normal distribution [3]:

$$f_{\Xi_h}(\xi_h) = \frac{1}{\sqrt{2\pi}\tilde{\sigma}_h \xi_h} \exp\left(-\frac{\log^2 \xi_h}{2\tilde{\sigma}_h^2}\right) \mathbb{1}_{\mathbb{R}_{>0}}(\xi_h), \tag{19}$$

where $\tilde{\sigma}_h$ is the shadowing standard deviation for the respective link state. The shadowing model is formulated adopting the independent shadowing assumption, according to which the ξ_h values on the different links may be reasonably considered independent, since the link correlations have a minor impact on the signal to interference-plus-noise ratio (SINR) distributions [33]. Observe that, as experimentally proved in [3], also directional LOS links may be subject to shadowing, since an optical LOS does not directly imply a clear radio wave LOS. Thus, when the first Fresnel zone around the direct link is partially obstructed by obstacles, statistical signal fluctuations might occur even in optical LOS conditions.

Small-scale fading measurements for the mmWave channel have been realized assuming a Rice distribution [5]. This distribution may be closely approximated by the Nakagami one [34, eq. 2.54], which is more suitable to provide analytical expressions when involved in integral calculations. Hence, the small-scale power fluctuations for LOS/NLOS links can be described, for $h = 1, 2$, through a gamma distributed rv Ψ_h having pdf:

$$f_{\Psi_h}(\psi_h) = \frac{m_h^{m_h}}{\Gamma(m_h)} \psi_h^{m_h-1} e^{-m_h \psi_h} \mathbb{1}_{\mathbb{R}_{\geq 0}}(\psi_h), \tag{20}$$

where $m_h (\geq 1/2)$ is the Nakagami parameter referred to the link state.

The final quantity that is included in the considered mmWave propagation environment is the noise power, which is evaluated at the receiver of D as [13]:

$$\sigma^2_{\mathcal{N}} = \mathcal{D}_{\mathcal{N}} \cdot B_{\mathrm{W}} \cdot \mathcal{K}_{\mathcal{N}}, \tag{21}$$

where $\mathcal{D}_{\mathcal{N}} \cong 3.98 \cdot 10^{-21}$ W/Hz is the noise spectral density, B_{W} is the receiver bandwidth, and $\mathcal{K}_{\mathcal{N}}$ is its noise figure. Differently from μWave networks, in which the noise can be often reasonably neglected, in the mmWave ones, the noise has a significant impact on the achievable performance and must be hence included in the analysis.

III. Problem Formulation

The system model introduced in the previous section accounts for many of the main elements that influence the result of a mmWave communication, thus it can be usefully employed to derive an accurate estimation of the coverage probability in the 2D and 3D scenarios for the target S_1-D communication. This problem can be formulated in more detail as follows.

Let consider the rv P_i, whose realization, representing the power p_i received by the destination D from the source S_i, may be expressed, for $i = 1, ..., L$, as:

$$p_i = \tilde{K} \left[\delta_{i1} \mathcal{G}_\nu^{\max} + (1 - \delta_{i1}) \mathfrak{g}_\nu\right] \cdot \begin{cases} 0 & \text{w.p. } f_{H|R_i}(0|r_i) \\ \dfrac{\xi_1 \psi_1}{\varrho_1(r_i)} & \text{w.p. } f_{H|R_i}(1|r_i) \\ \dfrac{\xi_2 \psi_2}{\varrho_2(r_i)} & \text{w.p. } f_{H|R_i}(2|r_i) \end{cases} \tag{22}$$

where $\tilde{K} = P_{\mathrm{T}} \mathcal{A}_1^{\max} \mathcal{A}_2^{\max}$ accounts for the transmission power and the maximum transmitting/receiving antenna gains. As specified in *Remark 1*, the rv U, denoting the overall interference received by D, is modeled by using the strongest interferer approximation [12], which estimates U as the maximum between the $L-1$ independent and identically distributed (i.i.d.) rvs $P_2, ..., P_L$. Therefore, the realization υ of the rv Υ, representing the SINR for the target link, is evaluated as:

$$\upsilon = \frac{p_1}{u + \sigma^2_{\mathcal{N}}}, \tag{23}$$

where:

$$u \cong \max(p_2, ..., p_L), \tag{24}$$

is the realization of U. According to [11], a communication may be assumed successful if its SINR is larger or equal to a SINR threshold ϖ, which models the effects of modulation, channel encoder, packet length, and desired packet error rate. Hence, given the ϖ value, the space dimension $\nu \in \mathbb{D}$, and the spatial distribution $d \in \mathbb{S}$, the coverage probability $\eta_{\nu,d}(\varpi|L)$ in the presence of L sources for the S_1-D communication may be obtained by evaluating at ϖ the complementary cdf (ccdf) $\bar{F}^{\nu,d}_{\Upsilon}(\upsilon|L)$ of Υ given L, that is:

$$\eta_{\nu,d}(\varpi|L) = \bar{F}^{\nu,d}_{\Upsilon}(\varpi|L). \tag{25}$$

The objective of the proposed analysis is that of theoretically estimating (25) for $\nu \in \mathbb{D}$ and $d \in \mathbb{S}$, preliminarily deriving the cdfs of (22)-(24). This task is accomplished in the next section.

IV. Analysis

The coverage analysis is developed by subdividing the entire procedure into four steps. In the first step, the impact of path-loss attenuation and small-scale fading is modeled for $\nu \in \mathbb{D}$ and $d \in \mathbb{S}$. In the second step, an estimation of the unconditional link-state probabilities is calculated. This result is the main approximation introduced in the analysis, where, however, the conditioning is removed taking into account the effect of the spatial statistic. In the third step, the cdf of P_i and the pdf of P_1 are determined by accounting for mid-scale fading and for the equivalent product gain. In the fourth step, the coverage probability in (25) is finally determined.

In more detail, the first step consists in evaluating the cdf of the rv $Q_{i,h}$ having realization:

$$q_{i,h} = \frac{\tilde{K} \psi_h}{\varrho_h(r_i)}, \quad i = 1, ..., L; \ h = 1, 2 \tag{26}$$

which accounts for path-loss attenuation and small-scale fading. According to (26), the cdf of $Q_{i,h}$ depends, by R_i, on the distance distribution, thus it is different for the UD, RW, and PPP spatial statistics. This allows the formulation of the three following lemmas.

Lemma 1 (Cdf of $Q_{i,h}$ for UD): Let R_i be distributed according to (4) and Ψ_h according to (20). Then, for $d = \mathrm{UD}$,

$$F^{\nu,\mathrm{UD}}_{Q_{i,h}}(q_{i,h}) = \frac{1}{\Gamma(m_h)} \left[\gamma\left(m_h, \frac{q_{i,h}}{\chi_h}\right) - \left(\frac{\chi_h}{q_{i,h}}\right)^{\frac{\nu}{\beta_h}} \gamma\left(m_h + \frac{\nu}{\beta_h}, \frac{q_{i,h}}{\chi_h}\right)\right] \mathbb{1}_{\mathbb{R}_{>0}}(q_{i,h}) \tag{27}$$

$$F^{\nu,\mathrm{RW}}_{Q_{i,h}}(q_{i,h}) = -\frac{1}{\Gamma(m_h)} \left[\sum_{k=0}^{\nu} a_{\nu,k} \left(\frac{\chi_h}{q_{i,h}}\right)^{\mu^k_{\nu,h}} \gamma\left(m_h + \mu^k_{\nu,h}, \frac{q_{i,h}}{\chi_h}\right)\right] \mathbb{1}_{\mathbb{R}_{>0}}(q_{i,h}) \tag{29}$$

$$\tilde{F}_{Q_h}^{\nu,\mathrm{PPP}}(q_h;\lambda)=\mathbb{1}_{\mathbb{R}_{>0}}(q_h)\cdot\begin{cases}\left(\dfrac{q_h}{q_h+\chi_h K_\nu \bar{R}^\nu\lambda}\right)^{m_h} & (\nu,\beta_h)\in\mathbf{C}_1\\ \displaystyle\sum_{k=0}^{2}\mathcal{B}_{\nu,k}(q_h,\lambda)\,{}_2F_2[\mathbf{b}_{\nu,k};\mathbf{c}_k;-\mathcal{E}_\nu(q_h,\lambda)] & (\nu,\beta_h)\in\mathbf{C}_2\end{cases} \tag{32}$$

$$\tilde{f}_H^{\nu,d,i}(h;\lambda)=\begin{cases}\max\left[0,1-\exp(\mathcal{K}_{\mathrm{out}})\,\mathcal{F}^{\nu,d}(\mathcal{H}_{\mathrm{out}}\bar{R};\lambda)\right] & h=0\\ \exp\left[\left[\tilde{f}_H^{\nu,d,i}(0;\lambda)\right]\mathcal{K}_{\mathrm{out}}\right]\mathcal{F}^{\nu,d}\left\{\left[\left[\tilde{f}_H^{\nu,d,i}(0;\lambda)\right]\mathcal{H}_{\mathrm{out}}+\mathcal{H}_{\mathrm{los}}\right]\bar{R};\lambda\right\} & h=1\\ 1-\displaystyle\sum_{h=0}^{1}\tilde{f}_H^{\nu,d,i}(h;\lambda) & h=2\end{cases} \tag{35}$$

$$\mathcal{F}^{2,d}(x;y)=\frac{2}{x^2}\cdot\begin{cases}\gamma(2,x) & d=\mathrm{UD}\\ \dfrac{x^2}{2}\left[1-\dfrac{x}{2\bar{R}\sqrt{y}}\exp\left(\dfrac{x^2}{4\pi\bar{R}^2y}\right)\mathrm{erfc}\left(\dfrac{x}{2\bar{R}\sqrt{\pi y}}\right)\right] & d=\mathrm{PPP}\\ \displaystyle\sum_{k=1}^{2}a_{2,k}kx^{2(1-k)}\,\gamma(2k,x) & d=\mathrm{RW}\end{cases} \tag{36}$$

$$\mathcal{F}^{3,d}(x;y)=\frac{3}{x^3}\cdot\begin{cases}\gamma(3,x) & d=\mathrm{UD}\\ \dfrac{x^3}{3}\left[{}_1F_2\left(1;\dfrac{1}{2},\dfrac{2}{3};-\dfrac{x^3}{36\pi\bar{R}^3y}\right)-\dfrac{1}{3}\sqrt[3]{\dfrac{2\pi^2}{y}}\mathrm{Bi}\left(-\dfrac{x}{\bar{R}\sqrt[3]{4\pi y}}\right)\right] & d=\mathrm{PPP}\\ \dfrac{1}{3}\displaystyle\sum_{k=1}^{3}a_{3,k}\,(2k{+}1)x^{2(1-k)}\,\gamma(2k{+}1,x) & d=\mathrm{RW}\end{cases} \tag{37}$$

$\nu\in\mathbb{D}$, $i=1,...,L$, $h=1,2$, the cdf of $Q_{i,h}$ is given by (27), shown at the bottom of the previous page, where:

$$\chi_h=\frac{\tilde{K}}{m_h\varrho_h(\bar{R})}. \tag{28}$$

Proof: See Appendix A-A. □

Lemma 2 (Cdf of $Q_{i,h}$ for RW): Let R_i be distributed according to (6) and Ψ_h according to (20). Then, for $d=\mathrm{RW}$, $\nu\in\mathbb{D}$, $i=1,...,L$, $h=1,2$, the cdf of $Q_{i,h}$ is given by (29), shown at the bottom of the previous page, where $a_{\nu,0}=-1$ and:

$$\mu_{\nu,h}^k=\frac{(1-\delta_{k0})\,\zeta_{\nu,k}}{\beta_h}. \tag{30}$$

Proof: See Appendix A-B. □

Lemma 3 (Cdf of $Q_{i,h}$ for PPP): Let R be distributed according to (10) and Ψ_h according to (20). Then, for $d=\mathrm{PPP}$, $\nu,\beta_h\in\mathbb{D}$, $i=1,...,L$, $h=1,2$, the cdf of $Q_{i,h}$ is given by:

$$F_{Q_{i,h}}^{\nu,\mathrm{PPP}}(q_{i,h})=\tilde{F}_{Q_h}^{\nu,\mathrm{PPP}}(q_{i,h};\lambda_1), \tag{31}$$

where, for $\lambda\in\Lambda$, the definition in (32) shown at the top of this page holds, in which $\mathbf{C}_1=\{(2,2),(3,3)\}$, $\mathbf{C}_2=\{(2,3),(3,2)\}$, and:

$$\mathcal{B}_{\nu,k}(x,y)=\left[\left(\frac{3}{2\bar{R}^4}\right)^{4-\nu}\bar{R}^{3\nu-2}\,\mathcal{E}_\nu(x,y)\right]^{\frac{(\nu-2)m_h+k}{3}}\cdot\frac{7k^2-15k+4}{2\nu\Gamma(m_h)}\,\Gamma\left(\frac{2k+\beta_h m_h}{3}\right), \tag{33a}$$

$$\mathbf{b}_{\nu,k}=\left(\frac{3k^2-5k+6}{12}+\frac{m_h}{\nu},\frac{13k-3k^2}{12}+\frac{m_h}{\nu}\right), \tag{33b}$$

$$\mathbf{c}_k=\left(\frac{2^k}{3},2-\frac{2^{2-k}}{3}\right), \tag{33c}$$

$$\mathcal{E}_\nu(x,y)=\left[\frac{4\bar{R}^6\,(\pi y)^{\beta_h}}{9^{3-\nu}}\left(\frac{\chi_h}{x}\right)^\nu\right]^{(-1)^\nu}. \tag{33d}$$

Proof: See Appendix A-C. □

The choice of not even considering the shadowing statistic in *Lemmas 1-3* is motivated by the impossibility of obtaining closed-forms for the cdf of the product between a gamma and a log-normal rv. The objective of this first step is in fact that of providing a set of analytical expressions that may be properly managed in the subsequent derivations, where mid-scale fading will be taken into account by suitable approximations. Besides, in *Lemma 3*, the evaluation is limited to the cases $\beta_h\in\{2,3\}$, which, according to the experimental values in [3, Table I],

TABLE I
ADOPTED PARAMETERS [2]–[6]

$\bar{R}$	100 m	$\hat{\sigma}_{\phi,2}$	10.5^o	$\mathcal{H}_{\rm los}$	14.9 $\rm mm^{-1}$	$\tilde{\sigma}_1$	5.8 dB
$P_{\rm T}$	1 W	$\hat{\sigma}_{\theta,1}$	9^o	α_1	61.4 dB	$\tilde{\sigma}_2$	8.7 dB
N	16	$\hat{\sigma}_{\theta,2}$	10.1^o	α_2	72.0 dB	m_h, $h=1,2$	3
$\mathcal{A}_n^{\max}$, $n=1,2$	N^2	$\mathcal{H}_{\rm out}$	33.3 $\rm mm^{-1}$	β_1	2.0	$B_{\rm W}$	1 GHz
$\hat{\sigma}_{\phi,1}$	2.5^o	$\mathcal{K}_{\rm out}$	5.2	β_2	2.9	$\mathcal{K}_{\mathcal{N}}$	10 dB

exactly model the LOS environment ($\beta_1 = 2$), and closely model the NLOS one ($\beta_2 \cong 3$).

Once the distribution of $Q_{i,h}$ is available for each spatial statistic, the second step of the analysis consists in calculating the unconditional link state probabilities corresponding to (17), since the conditioning of $f_{H|R_i}(h|r_i)$ on R_i complicates the analytical tractability of the problem because of the dependence between path-loss attenuation and link state probability. This step is accomplished through the following lemma.

Lemma 4 (Link state probabilities): Let $f_{H|R_i}(h|r_i)$ be distributed according to (17). Then, for $\nu \in \mathbb{D}$, $d \in \mathbb{S}$, $i=1,...,L$, the unconditional link state probabilities are given by:

$$f_H^{\nu,d,i}(h) = \tilde{f}_H^{\nu,d,i}(h;\lambda_1), \;\; h=0,1,2 \tag{34}$$

where, for $\lambda \in \Lambda$, the definition in (35) shown at the top of the previous page holds, in which the function $\mathcal{F}^{\nu,d}(x;y)$ is defined for $\nu=2$ and $\nu=3$, by (36) and (37), shown at the top of the previous page, respectively.

Proof: See Appendix A-D. □

Using this latter result, one can introduce in the analysis the simplifying hypothesis of independence between path-loss attenuation and link state probability. The effect of this approximation, which makes analytically tractable the mathematical derivation of the coverage probability, will be checked in the next section through independent Monte Carlo simulations. According to this approach, the received power in (22) may be hence approximated by:

$$p_i \cong [\delta_{i1}\mathcal{G}_\nu^{\max} + (1-\delta_{i1})\mathfrak{g}_\nu] \cdot \begin{cases} 0 & \text{w.p. } f_H^{\nu,d,i}(0) \\ \xi_1 q_{i,1} & \text{w.p. } f_H^{\nu,d,i}(1) \\ \xi_2 q_{i,2} & \text{w.p. } f_H^{\nu,d,i}(2) \end{cases} \tag{38}$$

in which the dependence between the $f_H^{\nu,d,i}(h)$ values and the $\rm S_i$-D distance is no more present. The cdf of the rv P_i corresponding to (38) and then the pdf of P_1 can be calculated by formulating the following proposition, which represents the third step of the analysis.

Proposition 1 (Power statistics): Let $\epsilon_h = \exp(\sqrt{3}\tilde{\sigma}_h)$ and Ξ_h be distributed according to (19), H according to (34)-(37), $Q_{i,h}$ according to (27)-(28) for $d=$ UD, to (29)-(30) for $d=$ RW, to (31)-(33) for $d=$ PPP. Then, for $\nu \in \mathbb{D}$, $d \in \mathbb{S}$, $i=1,...,L$, the cdf of P_i is estimated by (39), reported at the bottom of the page, while, for $i=1$, the pdf of P_1 is evaluated by (40), still shown at the bottom of this page, where $f_{Q_{1,h}}^{\nu,d}(q_{1,h})$ is the pdf of $Q_{1,h}$, which is given by the derivative of (27) for $d=$ UD, of (29) for $d=$ RW, and of (31) for $d=$ PPP.

Proof: See Appendix A-E. □

Remark 4: The statistics in (39)-(40) derive from two approximations. The first one consists in the usage of the unconditional link state probabilities in place of the conditional ones, which enable to model the effect of the link state by applying the mixture distribution. The second one consists in the application of the improved Gaussian approximation presented in [35], which is exploited to estimate the statistics of the product between $Q_{i,h}$ and the log-normal rv Ξ_h. No approximations are instead introduced for the antenna pattern, which is maintained exactly as it is. Concerning this latter aspect, it is worth to remark that, differently from [16] and in agreement with [20], (39) is derived to allow each interfering source to experience a different equivalent product gain. This overcomes the limit of the model in [16], which was instead developed assuming an identical equivalent product gain for all the undesired sources. □

The fourth step of the analysis may be now finally carried out to evaluate the coverage probability in (25). This quantity can be in fact estimated according to the following proposition.

Proposition 2 (Coverage probability): Let P_1 be distributed according to (40), $P_{i\neq 1}$ according to (39) for $i \neq 1$, and let the SINR be approximated by (23)-(24). Then, for $\nu \in \mathbb{D}$ and $d \in \mathbb{S}$, the coverage probability may be estimated as:

$$\eta_{\nu,d}(\varpi|L) \cong \int_0^{+\infty} \left[F_{P_{i\neq 1}}^{\nu,d}\left(\frac{p_1}{\varpi} - \sigma_{\mathcal{N}}^2 \right) \right]^{L-1} f_{P_1}^{\nu,d}(p_1) \mathrm{d}p_1. \tag{41}$$

Proof: See Appendix A-F. □

$$F_{P_i}^{\nu,d}(p_i) \cong f_H^{\nu,d,i}(0)\mathbb{1}_{\mathbb{R}_{\geq 0}}(p_i) + \frac{2}{3}\sum_{h=1}^{2} f_H^{\nu,d,i}(h) \sum_{n=-1}^{1} \frac{1}{4^{|n|}} \cdot \begin{cases} F_{Q_{i,h}}^{\nu,d}\left(\dfrac{p_i}{\mathcal{G}_\nu^{\max}\epsilon_h^n} \right) & i=1 \\ \displaystyle\int_0^1 F_{Q_{i,h}}^{\nu,d}\left(\frac{p_i}{\mathfrak{g}_\nu \epsilon_h^n} \right) f_{\mathcal{G}_\nu}(\mathfrak{g}_\nu)\mathrm{d}\mathfrak{g}_\nu & i \neq 1 \end{cases} \tag{39}$$

$$f_{P_1}^{\nu,d}(p_1) \cong f_H^{\nu,d,1}(0)\delta(p_1) + \frac{2}{3\mathcal{G}_\nu^{\max}} \sum_{h=1}^{2} f_H^{\nu,d,1}(h) \sum_{n=-1}^{1} \frac{1}{4^{|n|}\epsilon_h^n} f_{Q_{1,h}}^{\nu,d}\left(\frac{p_1}{\mathcal{G}_\nu^{\max}\epsilon_h^n} \right) \tag{40}$$

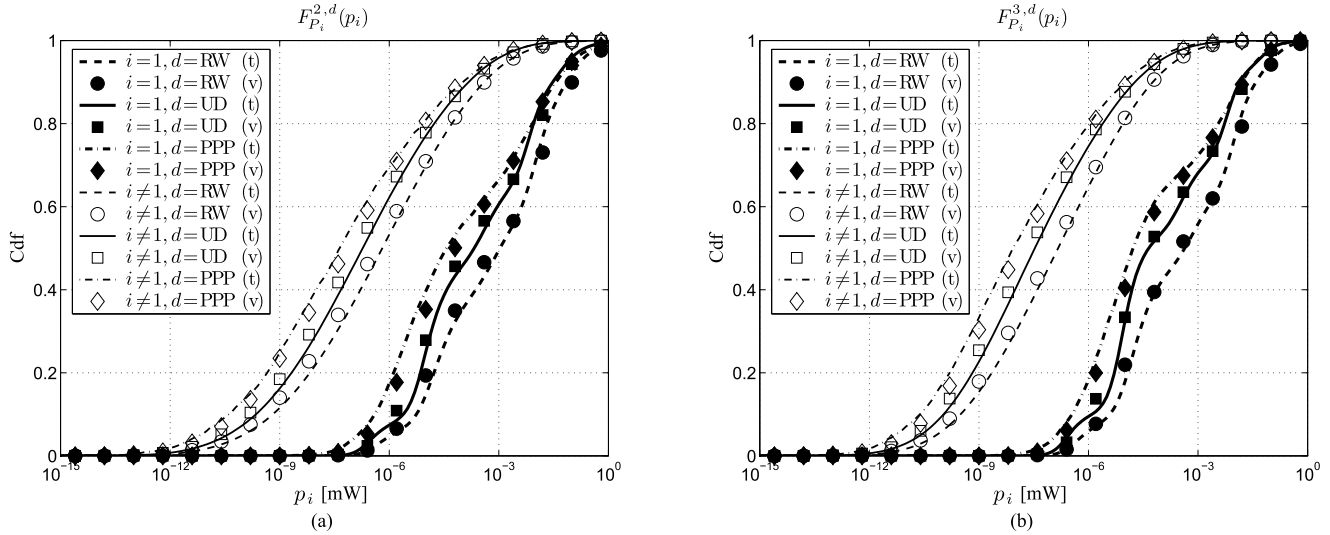

Fig. 2. Cdf of the power received from the desired ($i = 1$) and from a generic interfering ($i \neq 1$) source for different spatial statistics: (a) $\nu = 2$, (b) $\nu = 3$ (t: theory, v: Monte Carlo validation).

This latter result indicates that $\eta_{\nu,d}(\varpi|L)$ is influenced by the link conditions experienced not only by the desired source, but also by the undesired ones. Thus, the developed coverage analysis may be applied to both sparse and dense P2P networks, since (41) accounts for both interference and noise, and its derivation has not required the usage of the usually adopted noise-limited assumption. However, before describing some of the possible applications, the impact of the introduced approximations is investigated to check the accuracy of the developed model.

V. Results and Applications

The analysis is validated using the parameters in Table I, which refers to the measurements at 28 GHz reported in [2]–[6], and where N denotes the number of elements of the antenna array used by the communicating nodes. In particular, for the validation, the transmitting/receiving power gain patterns are selected identical and obtained from a broadside uniform square array lying on the $x-z$ plane and radiating in the y direction. The elements are spaced by a quarter of wavelength, thus providing, for $\nu \in \mathbb{D}$ and $n=1,2$, the pattern given by (42) [36], which is shown at the bottom of the page. Even if the proposed coverage analysis can manage any pattern shape, this array is selected for its wide practical usage [3], and for the availability of a well-established expression for the generated pattern that enables the possible reproducibility of the presented results.

Fig. 2 reports, for different spatial statistics, the cdf in (39) of the power received from the desired ($i = 1$) and from an interfering ($i \neq 1$) source in the 2D (Fig. 2(a)) and 3D (Fig. 2(b)) cases. The theoretical values (identified by lines) are validated by independent Monte Carlo simulations (identified by markers). This first set of results reveals that, both for $\nu = 2$ and $\nu = 3$, the destination statistically receives a higher power when the sources are located according to an RW model and a lower power when the sources are distributed according to a PPP. The UD presents an intermediate behavior. From the point of view of the model validation, the significant matching between analysis and simulations confirms the accuracy of the adopted mathematical approximations concerning the technique used to account for mid-scale fading and the adoption of the unconditional link state probabilities in place of the conditional ones. This feature is further corroborated by Fig. 3, which presents the coverage probability for different space dimensions and different spatial statistics as a function of the number of sources, considering the SINR thresholds $\varpi = 3$ dB (Fig. 3(a)) and $\varpi = 10$ dB (Fig. 3(b)). One may immediately infer from this figure that the choice of the spatial statistic may become a critical step when the purpose is to probabilistically estimate the result of a communication. In fact, some differences in terms of $\eta_{\nu,d}(\varpi|L)$ may be observed among the UD, RW, and PPP models, mainly for the 3D case, with the PPP that provides the lowest values. Another aspect that may be observed from Fig. 3 concerns the strong influence of the interference on the coverage probability, which suggests that the noise-limited approximation does not hold in the here addressed scenarios. A first application of the developed coverage analysis is indeed the deepening of this issue.

$$\mathcal{A}_n(\boldsymbol{\omega}_\nu) = \begin{cases} N \left| \dfrac{\sin(\sqrt{N}\pi \cos\phi_n/4)}{\sin(\pi\cos\phi_n/4)} \right|^2 & \nu = 2 \\ \left| \dfrac{\sin(\sqrt{N}\pi \sin\theta_n \cos\phi_n/4)\sin(\sqrt{N}\pi\cos\theta_n/4)}{\sin(\pi\sin\theta_n\cos\phi_n/4)\sin(\pi\cos\theta_n/4)} \right|^2 & \nu = 3 \end{cases} \tag{42}$$

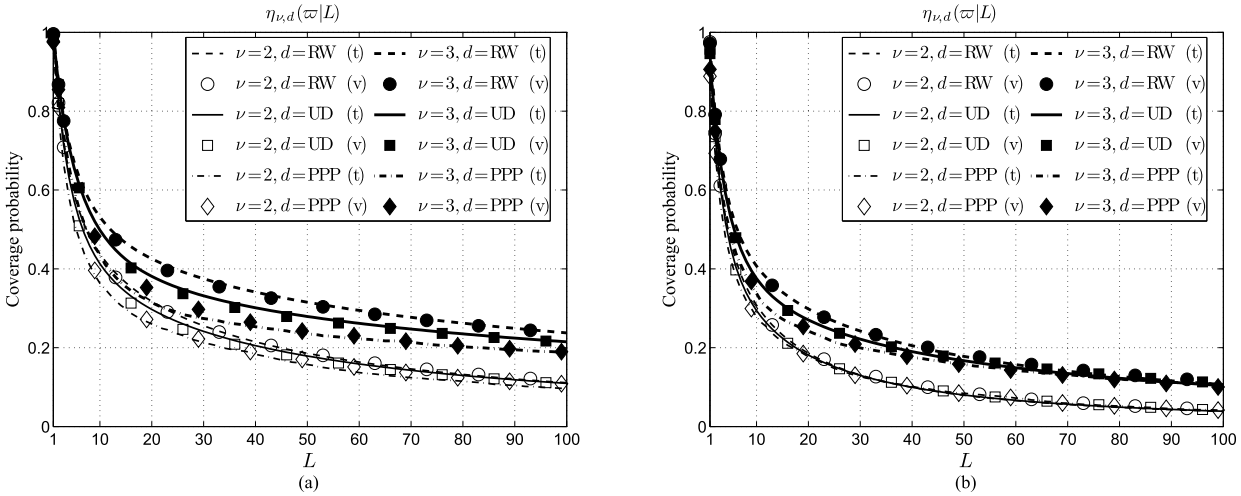

Fig. 3. Coverage probability for different space dimensions and spatial statistics as a function of the number of sources: (a) $\varpi = 3$ dB, (b) $\varpi = 10$ dB (t: theory, v: Monte Carlo validation).

A. Application 1: Concerning the Noise-Limited Approximation

The adoption of a pseudo-wired approximation for a directional communication in the presence of a Poisson field of interferers has been firstly proposed in [10], and further analyzed in [14], [15], by discussing the transitional behavior of mmWave networks from a noise-limited to an interference-limited regime. Differently from these studies, which have exhaustively addressed the influence of the network and channel parameters on the reliability of a noise-limited regime, our objective is to discuss if the approximations commonly introduced for modeling the interference may have a significant impact on the theoretically expected transitional behavior of mmWave networks. This issue is explored by comparing two common approaches: the strongest interferer approximation (SIA) [12], which, by (24), has been used in the here developed analysis, and the nearest interferer approximation (NIA) [13], which is more widely used and considers the closest interferer as the most harmful one. For this specific application, instead of using (42), which depends on the sole parameter N, a flat-top shape is adopted to separately control, for $n = 1, 2$, the two main parameters that characterize an antenna pattern: the main lobe beamwidth ϑ_n (measured in radians for $\nu = 2$ and in steradians for $\nu = 3$), and the backlobe gain $\mathcal{G}_{\mathrm{BL}_n}$. According to this choice, the pdf of the normalized equivalent transmitting ($n = 1$) and receiving ($n = 2$) gains may be expressed for $\nu \in \mathbb{D}$ as [13]:

$$f_{\mathcal{G}_{\nu,n}}(\mathfrak{g}_{\nu,n}) = \frac{\vartheta_n}{2^{\nu-1}\pi}\,\delta(\mathfrak{g}_{\nu,n}-1) + \left(1-\frac{\vartheta_n}{2^{\nu-1}\pi}\right)\delta(\mathfrak{g}_{\nu,n}-\mathcal{G}_{\mathrm{BL}_n}), \quad (43)$$

which, once inserted in the analysis, allows the formulation of the following proposition.

Proposition 3 (Coverage Probability/Beamwidth Relation): Let P_1 be distributed according to (40) with $\mathcal{G}_{\nu}^{\max} = 1$, Q_h according to (32)-(33) and H according to (35)-(37) for $\lambda \in \Lambda$, $\mathcal{G}_{\nu,n}$ according to (43) with $\mathcal{G}_{\mathrm{BL}_n} << 1$ for $n = 1, 2$. Then, for $\nu \in \mathbb{D}$ and $d = \mathrm{PPP}$, the coverage probability when $\lambda = \lambda_1$ (SIA) and $\lambda = \lambda_{L-1} = (L-1)\lambda_1$ (NIA) may be represented as (44), shown at the bottom of this page, where the function $\mathcal{Q}_\nu(x;\lambda)$ is given by (45), still shown at the bottom of this page.

Proof: See Appendix A-G. □

The consequences of this proposition may be inferred by recalling that, when the network is noise-limited, the interference must have a negligible effect on the coverage probability. Accordingly, in the presence of flat-top antennas with low backlobe gains, (44) states that, when the number of interferers increases and the beamwidths are given, the coverage probability gets away from its noise-limited value as $(\vartheta_1\vartheta_2)^{L-1}$ under the SIA, and as $\vartheta_1\vartheta_2$ under the NIA. This suggests that the NIA allows the adoption of less stringent antenna pattern requirements for satisfying the noise-limited assumption. This observation is confirmed by the results in Fig. 4, which are obtained using the parameters in Table I with $\mathcal{A}_1^{\max} = \mathcal{A}_2^{\max} = 20$ dB, $\nu = 3$, $\varpi = 10$ dB, and adopting the pattern in (43) with $\mathcal{G}_{\mathrm{BL}_1} = \mathcal{G}_{\mathrm{BL}_2} = \mathcal{G}_{\mathrm{BL}}$ and $\vartheta_1 = \vartheta_2 = \vartheta$. From now on, the simulations will be no more plotted to simplify the readability of the figures. These results clarify that a low backlobe gain and a moderately narrow beamwidth may be sufficient to allow the adoption of the noise-limited approximation when the NIA is adopted (Fig. 4(b)). Instead, under the SIA, the usage of a very narrow beamwidth becomes

$$\eta_{\nu,\mathrm{PPP}}(\varpi|L) \cong \int_0^{+\infty}\left[1-\vartheta_1\vartheta_2\mathcal{Q}_\nu\left(\frac{p_1}{\varpi}-\sigma_{\mathcal{N}}^2;\lambda\right)\right]^{\frac{\lambda_{L-1}}{\lambda}} f_{P_1}^{\nu,\mathrm{PPP}}(p_1)\mathrm{d}p_1 \quad (44)$$

$$\mathcal{Q}_\nu(x;\lambda) = \frac{2^{3-2\nu}}{3\pi^2}\sum_{h=1}^{2}\tilde{f}_H^{\nu,\mathrm{PPP},i\neq 1}(h;\lambda)\sum_{n=-1}^{1}\frac{1}{4^{|n|}}\left[1-\tilde{F}_{Q_h}^{\nu,\mathrm{PPP}}\left(\frac{x}{\epsilon_h^n};\lambda\right)\right] \quad (45)$$

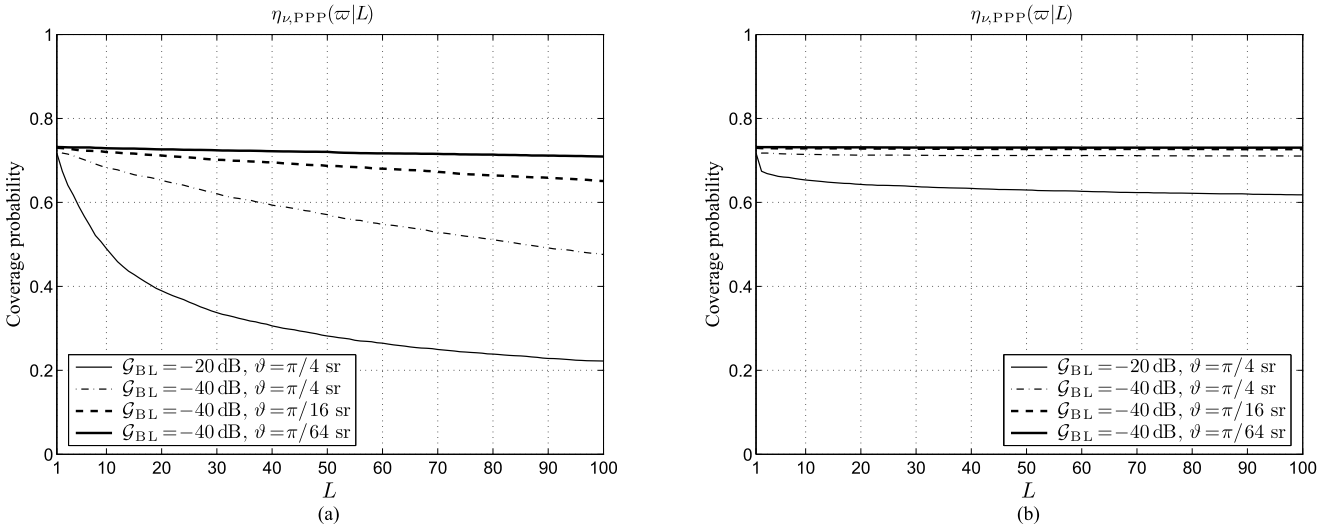

Fig. 4. Coverage probability as a function of the number of sources obtained using the flat-top antenna model for $\mathcal{A}_1^{\max}=\mathcal{A}_2^{\max}=20$ dB, $\nu=3$, $d=\mathrm{PPP}$, and $\varpi=10$ dB: (a) SIA, (b) NIA.

an additional requirement to make the noise-limited approximation acceptable (Fig. 4(a)). This reveals that the NIA can be useful to obtain analytically tractable models, but might result quite optimistic, with possible overestimations of the coverage probability and belief of being in a noise-limited regime when, instead, the antenna pattern is actually not enough directional for assuming that regime.

B. Application 2: Average Link Capacity in a P2P Network

The enabling of direct wireless links among different users represents one of the innovative features of forthcoming 5G cellular systems, in which a mobile mesh approach is thought as a mean to implement the recently conceived Internet of Things paradigm. Therefore, as a second application, the developed coverage analysis is used to estimate the average capacity of a communication link in a 3D ultra-dense (i.e., interference-limited) P2P network. In particular, handy closed-form expressions may be derived using a flat-top antenna model in a PPP-based scenario when all links are either in LOS or NLOS state (homogeneous link state conditions), and are not subject to small-scale fading (usually assumed less significant than shadowing in mmWave communications [13]). To this aim, a Poisson-distributed r.v. $\mathcal{L}$ is introduced to describe the number of active source-destination pairs. Accordingly, the pmf of $\mathcal{L}$ is given by:

$$f_{\mathcal{L}}(L)=\frac{\Delta^L}{L!}e^{-\Delta},\quad L=0,1,... \tag{46}$$

where Δ is the average number of active pairs. The capacity of each link is evaluated considering three cases: a limiting one, derived using the Shannon bound, and two based on a fixed binary phase-shift keying (BPSK) or quadrature PSK (QPSK) modulation. These two latter cases are modeled exploiting the expression derived in [37], which maintains for the capacity an approximation error lower than 1% for SINR values not too close to zero. Hence, by defining $\varsigma_1\cong 1.2860$, $\varsigma_2\cong 0.9308$, $\varsigma_3\cong 0.0102$ [37], the capacity of a generic communication link experiencing a SINR ϖ may be calculated for the three cases by the following expressions:

$$\mathcal{M}(\varpi)=\begin{cases}\log_2(1+\varpi) & \text{Shannon bound}\\ 1-\exp\left(-\varsigma_1\varpi^{\varsigma_2}+\varsigma_3\right) & \text{BPSK modulation}\\ 2-2\exp\left[-\varsigma_1\left(\frac{\varpi}{2}\right)^{\varsigma_2}+\varsigma_3\right] & \text{QPSK modulation}\end{cases} \tag{47}$$

which can be then exploited to formulate this final proposition.

Proposition 4 (Average link capacity): Let $\mathcal{L}$ be distributed according to (46), P_1 according to (40) with $\mathcal{G}_\nu^{\max}=1$, and $Q_{i,h}$ according to (31)-(33). Let $\mathcal{M}(\varpi)$ be given by (47) and $\eta_{\nu,\mathrm{PPP}}(\varpi|L)$ by (44)-(45), with $\lambda=\lambda_1$ (SIA), $\sigma^2_{\mathcal{N}}\cong 0$ (interference-limited scenario), $\vartheta_1\vartheta_2<<16\pi^2$ (highly directional links), and $f_H^{\nu,\mathrm{PPP},i}(h)=\tilde{f}_H^{\nu,\mathrm{PPP},i}(h;\lambda_1)=\delta_{h,1}\veebar\delta_{h,2}$ (homogeneous LOS/NLOS conditions). Then, for $\nu=3$ and $m_h\to+\infty$, the average link capacity may be approximated, for $h=1,2$, by:

$$\mathcal{C}_h(\varpi)\cong\mathcal{M}(\varpi)\left\{1-\frac{\vartheta_1\vartheta_2(\Delta-1)}{16\pi^2}\cdot\left[1-\frac{1}{18}\sum_{n=-2}^{2}\frac{2^{-\delta_{n,0}}(3-|n|)^2}{1+(\epsilon_h^n\varpi)^{\frac{3}{\beta_h}}}\right]\right\}. \tag{48}$$

Proof: See Appendix A-H. □

The results provided by (48) for $\vartheta_1=4\vartheta_2=\pi/4$ and $\Delta=10^3$ are reported in Fig. 5, which compares the average link capacity achievable in the 28 (Fig. 5(a)) and 73 (Fig. 5(b)) GHz bands using, for β_h and $\epsilon_h=\exp(\sqrt{3}\tilde{\sigma}_h)$, the values in [3, Table I]. This scenario, with a more directional antenna at the destination ($\vartheta_1>\vartheta_2$), models a possible 5G uplink interfered communication. The figure reveals that, for a given modulation and a given band, $\mathcal{C}_2(\varpi)>\mathcal{C}_1(\varpi)$, thus, when the link states are homogeneous, the NLOS condition for the interfering links is more advantageous than the LOS one for the target link. Besides, Fig. 5 puts into evidence the considerable gap between the ideal performance achievable through the Shannon bound and that actually provided by a fixed BPSK/QPSK modulation. One may also notice that the

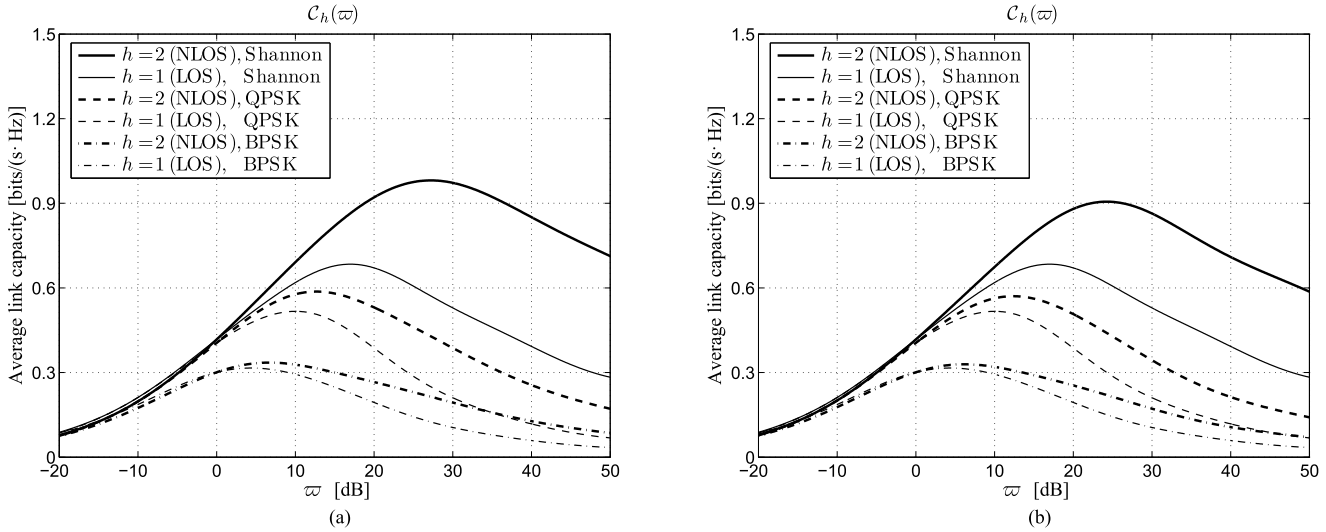

Fig. 5. Average link capacity as a function of the SINR for $\nu = 3$ using different modulations in homogeneous LOS/NLOS conditions: (a) 28 GHz band, (b) 73 GHz band.

difference in terms of capacity between the two bands is rather moderate. This confirms that, beside the antennas and the propagation environment, the interference remains determinant for establishing the link performance also in the mmWave context when an ultra-dense scenario is considered.

VI. Conclusion

A mathematical framework for estimating the coverage probability in 2D/3D P2P mmWave wireless networks has been presented. The developed model, which allows the maintenance of the actual antenna pattern during the analysis, has been derived considering different spatial statistics and realistic propagation conditions, compliant with recent channel measurements. By introducing suitable approximations to account for mid-scale fading and link state probabilities, simple integral formulas, validated through independent simulations, have been obtained.

The results have shown that, both for 2D and 3D networks, the RW spatial model leads to a higher received power as compared to the UD and PPP ones, and is preferable in terms of coverage probability. Besides, for a given number of active sources, the 2D scenario provides a lower coverage probability with respect to the 3D one, since, in this second case, the interferers are spread over a region having one more dimension. This aspect is relevant for 5G networks, where the usage of small cells can make the 3D performance of main interest. As a first application, the coverage analysis has been exploited to prove that, among the strongest and nearest interferer approximations, the latter one enables the transition towards a noise-limited regime with less stringent antenna pattern requirements, thus resulting potentially optimistic in estimating the actual interference. As a second application, an approximated closed-form estimation of the average link capacity in an ultra-dense interference-limited regime with homogeneous link states has been derived. This application has shown that, still in the mmWave domain, the interference plays a key role in characterizing the link performance.

As possible future developments, the conceived coverage analysis may be combined with the medium access control (MAC) scheme, so as to extend the discussion to point-to-multipoint communication scenarios and to the problem of initial access in 5G networks. In both these contexts, realistic multi-lobe antenna patterns may be already inserted in the proposed model, which, from the physical (PHY) layer point view, may be sufficiently general to allow the selection of the propagation phenomena that one intends to consider. For the proper assessment of both contexts, further research efforts are however required to move from the here presented single snapshot analysis, towards the investigation of the space-time interference correlation among different slots, with the final purpose of including the random access mechanism or the coordinated time division multiple access scheme into a complete mmWave MAC/PHY framework.

Appendix A

A. Proof of Lemma 1

Define the rv $\tilde{Q}_{i,h} = \tilde{K}/\varrho_h(R_i)$, whose cdf, by (18), can be calculated for $d \in \{\mathrm{UD}, \mathrm{RW}\}$ as:

$$F^{\nu,d}_{\tilde{Q}_{i,h}}(\tilde{q}_{i,h}) = \Pr\left\{\tilde{Q}_{i,h} \le \tilde{q}_{i,h}\right\} = 1 - F^{\nu,d}_{R_i}\left[\left(\frac{\tilde{K}}{\alpha_h \tilde{q}_{i,h}}\right)^{\frac{1}{\beta_h}}\right]. \quad (49)$$

By adopting (4) for the UD and using (28), (49) becomes:

$$F^{\nu,\mathrm{UD}}_{\tilde{Q}_{i,h}}(\tilde{q}_{i,h}) = \left[1 - \left(\frac{m_h \chi_h}{\tilde{q}_{i,h}}\right)^{\frac{\nu}{\beta_h}}\right] \mathbb{1}_{[m_h\chi_h, +\infty)}(\tilde{q}_{i,h}). \quad (50)$$

The cdf of $Q_{i,h} = \tilde{Q}_{i,h}\Psi_h$ may be then obtained for $d \in \mathbb{S}$ from the product distribution as [30]:

$$F^{\nu,d}_{Q_{i,h}}(q_{i,h}) = \int_0^{+\infty} F^{\nu,d}_{\tilde{Q}_{i,h}}\left(\frac{q_{i,h}}{\psi_h}\right) f_{\Psi_h}(\psi_h)\mathrm{d}\psi_h. \quad (51)$$

By inserting (20) and (50) in (51) and then solving the integral, one obtains (27).

B. Proof of Lemma 2

Similarly to *Lemma 1*, substitute (6) for $d = \mathrm{RW}$ in (49) and then use (28). This yields:

$$F^{\nu,\mathrm{RW}}_{\tilde{Q}_{i,h}}(\tilde{q}_{i,h}) = \left[1 - \sum_{k=1}^{\nu} a_{\nu,k} \left(\frac{m_h \chi_h}{\tilde{q}_{i,h}}\right)^{\frac{\zeta_{\nu,k}}{\beta_h}}\right] \mathbb{1}_{[m_h\chi_h,+\infty)}(\tilde{q}_{i,h}), \tag{52}$$

which, once inserted in (51) together with (20), provides (29) after integration. The parameter $a_{\nu,0}$ is added to those defined in (6) to obtain a compact representation of (29).

C. Proof of Lemma 3

Define the rv $\tilde{Q}_h = \tilde{K}/\varrho_h(R)$, whose cdf, by (10), (18), and (28), can be evaluated as:

$$\begin{aligned}\tilde{F}^{\nu,\mathrm{PPP}}_{\tilde{Q}_h}(\tilde{q}_h;\lambda) &= 1 - \tilde{F}^{\nu,\mathrm{PPP}}_{R}\left[\left(\frac{\tilde{K}}{\alpha_h \tilde{q}_h}\right)^{\frac{1}{\beta_h}};\lambda\right] \\ &= \exp\left[-\frac{K_\nu \lambda}{\bar{R}^{-\nu}}\left(\frac{m_h\chi_h}{\tilde{q}_h}\right)^{\frac{\nu}{\beta_h}}\right]\mathbb{1}_{\mathbb{R}_{>0}}(\tilde{q}_h). \end{aligned}\tag{53}$$

The cdf of $Q_h = \tilde{Q}_h \Psi_h$ obtainable by the product distribution:

$$\tilde{F}^{\nu,\mathrm{PPP}}_{Q_h}(q_h;\lambda) = \int_0^{+\infty} \tilde{F}^{\nu,\mathrm{PPP}}_{\tilde{Q}_h}\left(\frac{q_h}{\psi_h};\lambda\right) f_{\Psi_h}(\psi_h)\mathrm{d}\psi_h, \tag{54}$$

using (20) and (53) does not lead to closed-form expressions for all (ν, β_h) pairs. However, one may notice from [3, Table I] that, in LOS conditions, $\beta_1 = 2$, while, in NLOS conditions, $\beta_2 \cong 3$. Using these values in (54) together with (20), (54) may be analytically solved to derive, after some manipulations, (32) and (33). Recalling *Remark 1*, one finally obtains (31).

D. Proof of Lemma 4

Let consider the unconditional pdf:

$$\tilde{f}^{\nu,d,i}_{H}(h;\lambda) = \int_0^{+\infty} \mathrm{d}r_i\, f_{H|R_i}(h|r_i) \cdot \begin{cases} f^{\nu,d}_{R_i}(r_i) & d \in \{\mathrm{UD},\mathrm{RW}\} \\ \tilde{f}^{\nu,d}_{R_i}(r_i;\lambda) & d = \mathrm{PPP} \end{cases} \tag{55}$$

where $f_{H|R_i}(h|r_i)$ is given by (17), $f^{\nu,d}_{R_i}(r_i)$ by (3) for $d = \mathrm{UD}$ and by (5) for $d = \mathrm{RW}$, while $\tilde{f}^{\nu,d}_{R_i}(r_i;\lambda)$ is given by (11) for $d = \mathrm{PPP}$. The solution of the three integrals provides, after some algebra, (35)-(37). By recalling *Remark 1* for $d = \mathrm{PPP}$, and noticing, for $d \in \{\mathrm{UD},\mathrm{RW}\}$, that $\tilde{f}^{\nu,d,i}_{H}(h;\lambda)$ is independent of λ, one finally obtains (34).

E. Proof of Proposition 1

Define first the rv $W_{i,h} = Q_{i,h}\Xi_h$, where the cdf of $Q_{i,h}$ is provided by *Lemmas 1-3* for $d \in \mathbb{S}$ and the pdf of Ξ_h is given by (19). In this case, the product distribution does not lead to closed-forms. However, an accurate and computationally simple approximation for products involving normal, and also log-normal, rvs has been proposed in [35]. Using this approach, the cdf and pdf of $W_{i,h}$ may be approximated, respectively, by [35, eq. 5-7]:

$$F^{\nu,d}_{W_{i,h}}(w_{i,h}) \cong \frac{2}{3}\sum_{n=-1}^{1} \frac{1}{4^{|n|}} F^{\nu,d}_{Q_{i,h}}\left(\frac{w_{i,h}}{\epsilon^n_h}\right), \tag{56a}$$

$$f^{\nu,d}_{W_{i,h}}(w_{i,h}) \cong \frac{2}{3}\sum_{n=-1}^{1} \frac{1}{4^{|n|}\epsilon^n_h} f^{\nu,d}_{Q_{i,h}}\left(\frac{w_{i,h}}{\epsilon^n_h}\right). \tag{56b}$$

Then, according to (38), define the rv:

$$Z_i = \begin{cases} 0 & \text{w.p. } f^{\nu,d,i}_H(0) \\ W_{i,1} & \text{w.p. } f^{\nu,d,i}_H(1) \\ W_{i,2} & \text{w.p. } f^{\nu,d,i}_H(2) \end{cases} \tag{57}$$

whose cdf and pdf may be both evaluated by employing the mixture distribution as [38]:

$$F^{\nu,d}_{Z_i}(z_i) \cong \sum_{h=0}^{2} f^{\nu,d,i}_H(h) F^{\nu,d}_{W_{i,h}}(z_i), \tag{58a}$$

$$f^{\nu,d}_{Z_i}(z_i) \cong \sum_{h=0}^{2} f^{\nu,d,i}_H(h) f^{\nu,d}_{W_{i,h}}(z_i), \tag{58b}$$

in which the degenerate distribution $F^{\nu,d}_{W_{i,0}}(w_{i,0}) = \mathbb{1}_{\mathbb{R}_{\geq 0}}(w_{i,0})$ and its derivative $f^{\nu,d}_{W_{i,0}}(w_{i,0}) = \delta(w_{i,0})$ are introduced to account for the OUT state.

Consider now separately, in (38), the cases $i = 1$ and $i \neq 1$. For $i = 1$, $P_1 = \mathcal{G}^{\max}_{\nu} Z_1$ has cdf:

$$F^{\nu,d}_{P_1}(p_1) = F^{\nu,d}_{Z_1}\left(\frac{p_1}{\mathcal{G}^{\max}_{\nu}}\right), \tag{59}$$

and pdf:

$$f^{\nu,d}_{P_1}(p_1) = \frac{1}{\mathcal{G}^{\max}_{\nu}} f^{\nu,d}_{Z_1}\left(\frac{p_1}{\mathcal{G}^{\max}_{\nu}}\right). \tag{60}$$

For $i \neq 1$, the cdf of $P_i = \mathcal{G}_\nu Z_i$ derives from the product distribution as:

$$F^{\nu,d}_{P_i}(p_i) = \int_0^1 F^{\nu,d}_{Z_i}\left(\frac{p_i}{\mathfrak{g}_\nu}\right) f_{\mathcal{G}_\nu}(\mathfrak{g}_\nu)\mathrm{d}\mathfrak{g}_\nu. \tag{61}$$

Using (58a) and (56a) in (59) and (61), and then exploiting the linearity of the integral operator, one obtains (39). Similarly, using (58b) and (56b) in (60), one obtains (40).

F. Proof of Proposition 2

Since $P_2, ..., P_L$ are i.i.d., the cdf of U in (24) can be expressed as [30]:

$$F^{\nu,d}_{U}(u) \cong \left[F^{\nu,d}_{P_{i\neq 1}}(u)\right]^{L-1}. \tag{62}$$

Now, defining $f^{\nu,d}_U(u) = \mathrm{d}F^{\nu,d}_U(u)/\mathrm{d}u$ and exploiting (23) and (62), the ccdf of Υ in (23) may be obtained from the

$$f_{P_1}^{\nu,\mathrm{PPP}}(p_1) = \frac{2\tilde{\chi}_h^{\frac{\nu}{\beta_h}}}{\beta_h}\left\{\sum_{n=-1}^{1}\frac{\epsilon_h^{\frac{\nu n}{\beta_h}}}{4^{|n|}}\exp\left[-\left(\frac{\tilde{\chi}_h\epsilon_h^n}{p_1}\right)^{\frac{\nu}{\beta_h}}\right]\right\}\mathbb{1}_{\mathbb{R}_{>0}}(p_1). \tag{70}$$

$$\begin{aligned}\eta_{\nu,\mathrm{PPP}}^h(\varpi|L) &\cong \int_0^{+\infty}\left\{1-\frac{\vartheta_1\vartheta_2}{16\pi^2}\left[1-\frac{2}{3}\sum_{n=-1}^{1}\frac{1}{4^{|n|}}F_{Q_{i,h}}^{\nu,\mathrm{PPP}}\left(\frac{p_1}{\varpi}\right)\right]\right\}^{L-1} f_{P_1}^{\nu,\mathrm{PPP}}(p_1)\mathrm{d}p_1\\ &\cong 1-\frac{\vartheta_1\vartheta_2(L-1)}{16\pi^2}\left[1-\frac{2}{3}\sum_{n=-1}^{1}\frac{1}{4^{|n|}}\int_0^{+\infty}F_{Q_{i,h}}^{\nu,\mathrm{PPP}}\left(\frac{p_1}{\varpi}\right)f_{P_1}^{\nu,\mathrm{PPP}}(p_1)\mathrm{d}p_1\right],\end{aligned} \tag{71}$$

ratio distribution as [30]:

$$\begin{aligned}\bar{F}_{\Upsilon}^{\nu,d}(\upsilon|L) &= \Pr\{\Upsilon\geq\upsilon\} = \Pr\left\{U\leq\frac{P_1}{\upsilon}-\sigma_{\mathcal{N}}^2\right\}\\ &= \int_0^{+\infty}\left[\int_0^{\frac{p_1}{\upsilon}-\sigma_{\mathcal{N}}^2} f_U^{\nu,d}(u)\mathrm{d}u\right]f_{P_1}^{\nu,d}(p_1)\mathrm{d}p_1\\ &= \int_0^{+\infty}F_U^{\nu,d}\left(\frac{p_1}{\upsilon}-\sigma_{\mathcal{N}}^2\right)f_{P_1}^{\nu,d}(p_1)\mathrm{d}p_1\\ &\cong \int_0^{+\infty}\left[F_{P_{i\neq1}}^{\nu,d}\left(\frac{p_1}{\upsilon}-\sigma_{\mathcal{N}}^2\right)\right]^{L-1}f_{P_1}^{\nu,d}(p_1)\mathrm{d}p_1,\end{aligned} \tag{63}$$

which, once evaluated at $\upsilon=\varpi$, provides (41).

G. Proof of Proposition 3

As a first step, observe that, for $d=\mathrm{PPP}$ and $i\neq1$, $F_{P_i}^{\nu,d}(p_i)$ in (39) may be generalized to obtain $\tilde{F}_{P_i}^{\nu,\mathrm{PPP}}(p_i;\lambda)$ for $\lambda\in\Lambda$. This task can be accomplished repeating the proof of *Proposition 1* by using (32) in place of (31) and (35) in place of (34), thus formally obtaining (39) with the replacements $f_H^{\nu,d,i}(h)\rightarrow\tilde{f}_H^{\nu,\mathrm{PPP},i}(h;\lambda)$ and $F_{Q_{i,h}}^{\nu,d}\left(\frac{p_i}{\mathfrak{g}_\nu\epsilon_h^n}\right)\rightarrow\tilde{F}_{Q_h}^{\nu,\mathrm{PPP}}\left(\frac{p_i}{\mathfrak{g}_\nu\epsilon_h^n};\lambda\right)$. For $i=1$, (40) still holds, since the intensity of the PPP that models the location of the desired source is equal to λ_1 regardless of the adopted interference approximation (SIA or NIA).

As a second step, evaluate the pdf of the equivalent product gain by inserting (43) in (16). Recalling the properties of the Dirac delta function, this operation leads to:

$$\begin{aligned}f_{\mathcal{G}_\nu}(\mathfrak{g}_\nu) = \sum_{n,n'=0}^{1}\Bigg[&\left(\frac{\vartheta_1}{2^{\nu-1}\pi}\right)^{1-n}\left(\frac{\vartheta_2}{2^{\nu-1}\pi}\right)^{1-n'}\left(1-\frac{\vartheta_1}{2^{\nu-1}\pi}\right)^{n}\\ &\cdot\left(1-\frac{\vartheta_2}{2^{\nu-1}\pi}\right)^{n'}\delta(\mathfrak{g}_\nu-\mathcal{G}_{\mathrm{BL}_1}^n\mathcal{G}_{\mathrm{BL}_2}^{n'})\Bigg],\end{aligned} \tag{64}$$

which, for $\mathcal{G}_{\mathrm{BL}_1},\mathcal{G}_{\mathrm{BL}_2}<<1$, can be expressed as:

$$f_{\mathcal{G}_\nu}(\mathfrak{g}_\nu)\cong\frac{\vartheta_1\vartheta_2}{(2^{\nu-1}\pi)^2}\left[\delta(\mathfrak{g}_\nu-1)-\delta(\mathfrak{g}_\nu)\right]+\delta(\mathfrak{g}_\nu). \tag{65}$$

As a third step, substitute (65) in $\tilde{F}_{P_i}^{\nu,\mathrm{PPP}}(p_i;\lambda)$ for $i\neq1$, thus obtaining:

$$\tilde{F}_{P_{i\neq1}}^{\nu,\mathrm{PPP}}(p_i;\lambda)\cong1-\vartheta_1\vartheta_2\mathcal{Q}_\nu(p_i;\lambda), \tag{66}$$

where $\mathcal{Q}_\nu(x;\lambda)$ is given by (45). Consider now, separately, the SIA and NIA cases. Under the SIA, that is, for $\lambda=\lambda_1$, the coverage probability can be estimated repeating the proof of *Proposition 2* by using $\tilde{F}_{P_{i\neq1}}^{\nu,\mathrm{PPP}}(p_i;\lambda_1)$ in place of $F_{P_{i\neq1}}^{\nu,d}(p_i)$ in (63), which yields:

$$\begin{aligned}\bar{F}_{\Upsilon}^{\nu,\mathrm{PPP}}(\upsilon|L)\cong\int_0^{+\infty}\Bigg\{&\left[F_{P_{i\neq1}}^{\nu,\mathrm{PPP}}\left(\frac{p_1}{\upsilon}-\sigma_{\mathcal{N}}^2;\lambda_1\right)\right]^{L-1}\\ &\cdot f_{P_1}^{\nu,\mathrm{PPP}}(p_1)\Bigg\}\mathrm{d}p_1.\end{aligned} \tag{67}$$

Under the NIA, that is, for $\lambda=\lambda_{L-1}=(L-1)\lambda_1$, just the closest interferer must be taken into account, thus $U\cong P_{i\neq1}$ and hence $F_U^{\nu,d}(u)\cong\tilde{F}_{P_{i\neq1}}^{\nu,\mathrm{PPP}}(p_i;\lambda_{L-1})$. This modification may be inserted in the last step of (63), thus obtaining:

$$\begin{aligned}\bar{F}_{\Upsilon}^{\nu,d\mathrm{PPP}}(\upsilon|L)\cong\int_0^{+\infty}\Bigg\{&F_{P_{i\neq1}}^{\nu,\mathrm{PPP}}\left(\frac{p_1}{\upsilon}-\sigma_{\mathcal{N}}^2;\lambda_{L-1}\right)\\ &\cdot f_{P_1}^{\nu,\mathrm{PPP}}(p_1)\Bigg\}\mathrm{d}p_1.\end{aligned} \tag{68}$$

By evaluating (67) and (68) at $\upsilon=\varpi$ and then using (66), one finally obtains (44).

H. Proof of Proposition 4

As a first step, calculate, for $m_h\rightarrow+\infty$, the cdf of $Q_{i,h}$ from (53) and (28) as:

$$\begin{aligned}F_{Q_{i,h}}^{\nu,\mathrm{PPP}}(q_{i,h}) &= \tilde{F}_{\tilde{Q}_h}^{\nu,\mathrm{PPP}}(q_{i,h};\lambda_1)\\ &= \exp\left[-\left(\frac{\tilde{\chi}_h}{q_{i,h}}\right)^{\frac{\nu}{\beta_h}}\right]\mathbb{1}_{\mathbb{R}_{>0}}(q_{i,h}),\end{aligned} \tag{69}$$

where $\tilde{\chi}_h=\tilde{K}/\varrho_h(\bar{R})$. Now, using the derivative of (69) in (40) with $\mathcal{G}_\nu^{\max}=1$ and $f_H^{\nu,\mathrm{PPP},i}(h)=\delta_{h,1}\veebar\delta_{h,2}$, evaluate the pdf of P_1, thus obtaining (70), shown at the top of the page.

As a second step, consider (44)-(45) for $\lambda=\lambda_1$, $\sigma_{\mathcal{N}}^2\cong0$, $\tilde{f}_H^{\nu,\mathrm{PPP},i}(h;\lambda_1)=\delta_{h,1}\veebar\delta_{h,2}$, and $\vartheta_1\vartheta_2<<16\pi^2$, which, after some manipulations, lead, for $h=1,2$, to (71), still reported at the top of the page, where the latter expression derives from the binomial approximation.

As a third step, remove the conditioning of $\eta_{\nu,\mathrm{PPP}}^h(\varpi|L)$ with respect to $\mathcal{L}$ according to (46) and then multiply by $\mathcal{M}(\varpi)$ in (47), so as to estimate, for $h=1,2$, the average link capacity by:

$$\mathcal{C}_h(\varpi)=\mathcal{M}(\varpi)\cdot\left[\sum_{L=1}^{+\infty}\eta_{\nu,\mathrm{PPP}}^h(\varpi|L)f_{\mathcal{L}}(L)\right]. \tag{72}$$

By substituting (69)-(70) in (71), solving the corresponding integral, and then inserting the derived expression in (72), one finally obtains (48) for $\nu=3$.

REFERENCES

[1] J. G. Andrews *et al.*, "What will 5G be?" *IEEE J. Sel. Areas Commun.*, vol. 32, no. 6, pp. 1065–1082, Jun. 2014.

[2] T. A. Thomas, H. C. Nguyen, G. R. MacCartney, Jr., and T. S. Rappaport, "3D mmWave channel model proposal," in *Proc. IEEE VTC-Fall*, Sep. 2014, pp. 1–6.

[3] M. R. Akdeniz *et al.*, "Millimeter wave channel modeling and cellular capacity evaluation," *IEEE J. Sel. Areas Commun.*, vol. 32, no. 6, pp. 1164–1179, Jun. 2014.

[4] M. K. Samimi and T. S. Rappaport, "3-D statistical channel model for millimeter-wave outdoor mobile broadband communications," in *Proc. IEEE ICC*, Jun. 2015, pp. 2430–2436.

[5] M. K. Samimi, G. R. MacCartney, Jr., S. Sun, and T. S. Rappaport, "28 GHz millimeter-wave ultrawideband small-scale fading models in wireless channels," in *IEEE VTC Spring*, May 2016, pp. 1–6.

[6] M. K. Samimi and T. S. Rappaport, "3-D millimeter-wave statistical channel model for 5G wireless system design," *IEEE Trans. Microw. Theory Techn.*, vol. 64, no. 7, pp. 2207–2225, Jul. 2016.

[7] *IEEE Std for HR WPANs MAC/PHY Specif. Amend. 2: mmWave Based Alternative PHY Ext*, IEEE Standard 802.15.3c, Oct. 2009.

[8] *IEEE Std for WLAN MAC/PHY Specif. Amend. 3: Enhanc. VHT in the 60 GHz Band*, IEEE Standard 802.11ad, 2014.

[9] *IEEE Standard for WirelessMAN-Advanced Air Interface for Broadband Wireless Access Systems*, IEEE Standard 802.16.1, Sep. 2012.

[10] S. Singh, R. Mudumbai, and U. Madhow, "Interference analysis for highly directional 60-GHz mesh networks: The case for rethinking medium access control," *IEEE/ACM Trans. Netw.*, vol. 19, no. 5, pp. 1513–1527, Oct. 2011.

[11] T. Bai and R. W. Heath, Jr., "Coverage and rate analysis for millimeter-wave cellular networks," *IEEE Trans. Wireless Commun.*, vol. 14, no. 2, pp. 1100–1114, Feb. 2015.

[12] F. Babich and M. Comisso, "A reliable approach for modeling the actual antenna pattern in millimeter-wave communication," *IEEE Commun. Lett.*, vol. 19, no. 8, pp. 1335–1338, Aug. 2015.

[13] M. Di Renzo, "Stochastic geometry modeling and analysis of multi-tier millimeter wave cellular networks," *IEEE Trans. Wireless Commun.*, vol. 14, no. 9, pp. 5038–5057, Sep. 2015.

[14] H. Shokri-Ghadikolaei *et al.*, "Millimeter wave cellular networks: A MAC layer perspective," *IEEE Trans. Commun.*, vol. 63, no. 10, pp. 3437–3458, Oct. 2015.

[15] H. Shokri-Ghadikolaei and C. Fischione, "The transitional behavior of interference in millimeter wave networks and its impact on medium access control," *IEEE Trans. Commun.*, vol. 64, no. 2, pp. 723–740, Feb. 2016.

[16] F. Babich, M. Comisso, and A. Cuttin, "Uplink capacity of interfered millimeter-wave communications: 3D theoretical analysis," in *Proc. IEEE GLOBECOM*, Dec. 2016, pp. 1–6.

[17] F. Babich, M. Comisso, and A. Cuttin, "Impact of interference spatial distribution on line-of-sight millimeter-wave communications," in *Proc. VDE Eur. Wireless*, May 2017, pp. 1–6.

[18] J. G. Andrews, T. Bai, M. N. Kulkarni, A. Alkhateeb, A. K. Gupta, and R. W. Heath, Jr., "Modeling and analyzing millimeter wave cellular systems," *IEEE Trans. Commun.*, vol. 65, no. 1, pp. 403–430, Jan. 2017.

[19] V. M. Nguyen and M. Kountouris, "Performance limits of network densification," *IEEE J. Sel. Areas Commun.*, vol. 35, no. 6, pp. 1294–1308, Mar. 2017.

[20] X. Yu, J. Zhang, M. Haenggi, and K. B. Letaief, "Coverage analysis for millimeter wave networks: The impact of directional antenna arrays," *IEEE J. Sel. Areas Commun.*, vol. 35, no. 7, pp. 1498–1512, Jul. 2017.

[21] M. Cheng, J.-B. Wang, Y. Wu, X.-G. Xia, K.-K. Wong, and M. Lin, "Coverage analysis for millimeter wave cellular networks with imperfect beam alignment," *IEEE Trans. Veh. Technol.*, vol. 67, no. 9, pp. 8302–8314, Sep. 2018.

[22] V. Mordachev and S. Loyka, "On node density—Outage probability tradeoff in wireless networks," *IEEE J. Sel. Areas Commun.*, vol. 27, no. 7, pp. 1120–1131, Sep. 2009.

[23] S. Srinivasa and M. Haenggi, "Distance distributions in finite uniformly random networks: Theory and applications," *IEEE Trans. Veh. Technol.*, vol. 59, no. 2, pp. 940–949, Feb. 2010.

[24] V. Naghshin, A. M. Rabiei, N. C. Beaulieu, and B. Maham, "Accurate statistical analysis of a single interference in random networks with uniformly distributed nodes," *IEEE Commun. Lett.*, vol. 18, no. 2, pp. 197–200, Feb. 2014.

[25] Z. Gong and M. Haenggi, "Interference and outage in mobile random networks: Expectation, distribution, and correlation," *IEEE Trans. Mobile Comput.*, vol. 13, no. 2, pp. 337–349, Feb. 2014.

[26] F. Babich and M. Comisso, "Including the angular domain in the analysis of finite multi-packet peer-to-peer networks with uniformly distributed sources," *IEEE Trans. Commun.*, vol. 64, no. 6, pp. 2494–2510, Jun. 2016.

[27] C. Bettstetter, G. Resta, and P. Santi, "The node distribution of the random waypoint mobility model for wireless ad hoc networks," *IEEE Trans. Mobile Comput.*, vol. 2, no. 3, pp. 257–269, Jul. 2003.

[28] E. Hyytiä and J. Virtamo, "Random waypoint model in n-dimensional space," Netw. Lab., Univ. Helsinki, Helsinki, Finland, Tech. Rep. COST279TD(04)032, Sep. 2004.

[29] H. R. Thompson, "Distribution of distance to Nth neighbour in a population of randomly distributed individuals," *Ecology*, vol. 37, no. 2, pp. 391–394, Apr. 1956.

[30] R. D. Yates and D. J. Goodman, *Probability and Stochastic Processes*. New York, NY, USA: Wiley, 1999.

[31] C. Bettstetter, H. Hartenstein, and X. Pérez-Costa, "Stochastic properties of the random waypoint mobility model," *Wireless Netw.*, vol. 10, no. 5, pp. 555–567, Sep. 2004.

[32] *Further Advancements for E-UTRA Physical Layer Aspects*, document 3GPP TR 36.814 (Rel.9), Mar. 2010.

[33] T. Bai, R. Vaze, and R. W. Heath, Jr., "Analysis of blockage effects on urban cellular networks," *IEEE Trans. Wireless Commun.*, vol. 13, no. 9, pp. 5070–5083, Sep. 2014.

[34] G. L. Stüber, *Principles of Mobile Communication*. Norwell MA, USA: Kluwer, 1996.

[35] J. M. Holtzman, "A simple, accurate method to calculate spread-spectrum multiple-access error probabilities," *IEEE Trans. Commun.*, vol. 40, no. 3, pp. 461–464, Mar. 1992.

[36] C. A. Balanis, *Antenna Theory: Analysis and Design*. New York, NY, USA: Wiley, 1997.

[37] F. Babich *et al.*, "Useful mathematical tools for capacity approaching codes design," *IEEE Commun. Lett.*, vol. 21, no. 9, pp. 1949–1952, Sep. 2017.

[38] S. Frühwirth-Schnatter, *Finite Mixture and Markov Switching Models*. New York, NY, USA: Springer, 2006.

Massimiliano Comisso (M'09) received the Laurea degree in electronic engineering and the Ph.D. degree in information engineering from the University of Trieste, Italy. He was with Alcatel, where he was engaged in DWDM communication systems, and collaborated with Danieli Automation on electromagnetic NDE techniques. He is currently an Assistant Professor with the Department of Engineering and Architecture, University of Trieste. He has authored/coauthored more than 70 international scientific papers. His research interests include distributed wireless networks, millimeter wave communications, antenna array synthesis, and small antennas. He serves as a referee/TPC member for several IEEE journals and conferences. He has been the Best Student Paper Award Finalist at GLOBECOM 2006 and received the Best Paper Award at CAMAD 2009.

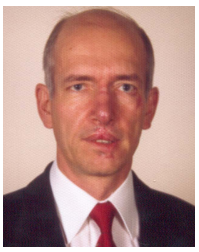

Fulvio Babich (SM'02) received the doctoral degree (Laurea), *(cum laude)*, in electrical engineering from the University of Trieste, in 1984. After graduation, he was with the Research and Development Laboratories, Telettra, where he was engaged in optical fiber communications. Then he joined Zeltron, where he was a Communication System Engineer, responsible for the activities within the ESPRIT program. In 1992, he joined the Department of Electrical Engineering (DEEI), University of Trieste, where he is currently a Professor in digital communications and wireless networks. He is also the Vice Director of the Department of Engineering and Architecture, and he has been recently elected as the Coordinator of the Ph.D. program for Industrial and Information Engineering of the University of Trieste. His current research interests include wireless networks and millimeter wave communications. He is involved in channel modeling, multiple access techniques, channel encoding, error control techniques, and cross-layer design. He is a member of the Board of the National Telecommunications and Information Theory Group - GTTI and was a member of the Directive Board of CNIT (National Inter-University Consortium for Telecommunications).